Addiction-associated genetic variants implicate brain cell type- and region-specific cis-regulatory elements in addiction neurobiology

Chaitanya Srinivasan[1*], BaDoi N. Phan[1,2*], Alyssa J. Lawler[3], Easwaran Ramamurthy[1], Michael Kleyman[1], Ashley R. Brown[1], Irene M. Kaplow[1,4], Morgan E. Wirthlin[1,4], Andreas R. Pfenning[1,3,4,‡]

[1]Computational Biology Department, School of Computer Science, Carnegie Mellon University, 15213
[2]Medical Scientist Training Program, School of Medicine, University of Pittsburgh, 15213
[3]Department of Biological Sciences, Mellon College of Science, Carnegie Mellon University, 15213
[4]Neuroscience Institute, Carnegie Mellon University, 15213
[*]CS and BNP contributed equally to the work
[‡]Direct correspondence to apfenning@cmu.edu

Number of pages: 54 pages of text, 13 pages of figures

Number of figures:
- 5 main figures
- 6 supplemental figures
- 1 supplemental table

Number of words
- Abstract: 244 words
- Introduction: 559 words
- Discussion: 1347 words

CONFLICT OF INTEREST:
AJL, ER, and ARP are inventors of the cSNAIL patent. Other authors do not declare any conflict of interest.

ACKNOWLEDGEMENT

We would like to thank members of the Eric Yttri lab at Carnegie Mellon University for providing *Drd1-cre* and *Adora2a-cre* mice for cell type-specific ATAC-seq experiments.

Author contributions: Conceptualization: ARP, BNP, CS; ATAC-seq data processing: AJL, ER, IMK, BNP; GWAS enrichment investigation: BNP, CS, ER, MK; Machine learning models: AJL, BNP, ER, IMK; bulk tissue ATAC-seq: AJL, ARB, MEW; cSNAIL ATAC-seq: AJL, ARB; writing (original draft): BNP, CS; review and editing: AJL, ARP, BNP, CS, ER, IMK; funding acquisition, resources, & supervision: ARP;

Funding: National Institute of General Medical Sciences training grant T32GM008208 (BNP), Sloan Foundation Fellowship (ARP), National Institute on Drug Abuse Avenir Award 1DP1DA046585 (ARP), National Science Foundation Graduate Student Research Fellowship DGE1745016 (AJL), Carnegie Mellon Brainhub Presidential Fellowship (ER), Carnegie Mellon Computational Biology Department Lane Postdoctoral Fellowship (IMK)

ABSTRACT

Recent large genome-wide association studies (GWAS) have identified multiple confident risk loci linked to addiction-associated behavioral traits. Genetic variants linked to addiction-associated traits lie largely in non-coding regions of the genome, likely disrupting cis-regulatory element (CRE) function. CREs tend to be highly cell type-specific and may contribute to the functional development of the neural circuits underlying addiction. Yet, a systematic approach for predicting the impact of risk variants on the CREs of specific cell populations is lacking. To dissect the cell types and brain regions underlying addiction-associated traits, we applied LD score regression to compare GWAS to genomic regions collected from human and mouse assays for open chromatin, which is associated with CRE activity. We found enrichment of addiction-associated variants in putative regulatory elements marked by open chromatin in neuronal (NeuN+) nuclei collected from multiple prefrontal cortical areas and striatal regions known to play major roles in reward and addiction. To further dissect the cell type-specific basis of addiction-associated traits, we also identified enrichments in human orthologs of open chromatin regions of mouse neuron subtypes: cortical excitatory, PV, D1, and D2. Lastly, we developed machine learning models from mouse cell type-specific regions of open chromatin to further dissect human NeuN+ open chromatin regions into cortical excitatory or striatal D1 and D2 neurons and predict the functional impact of addiction-associated genetic variants. Our results suggest that different neuron subtypes within the reward system play distinct roles in the variety of traits that contribute to addiction.

Significance Statement:

Our study on cell types and brain regions contributing to heritability of addiction-associated traits suggests that the conserved non-coding regions within cortical excitatory and striatal medium

68 spiny neurons contribute to genetic predisposition for nicotine, alcohol, and cannabis use
69 behaviors. This computational framework can flexibly integrate epigenomic data across species to
70 screen for putative causal variants in a cell type- and tissue-specific manner across numerous
71 complex traits.

INTRODUCTION

Substance use disorders (SUD) have increased in prevalence over the last three decades, with an estimated 100 million cases worldwide(GBD 2016 Alcohol and Drug Use Collaborators, 2018; Eddie et al., 2019). Pharmacological interventions are limited in their ability to cure addiction due to physiological and logistical barriers(Pullen and Oser, 2014; Pear et al., 2019). As the societal epidemic of substance use grows, there is a greater need to understand the neurobiology of substance use behaviors and addiction.

The reward circuits co-opted in addiction are highly conserved across primates and rodents(Scaplen and Kaun, 2016). It is generally accepted that addictive substances promote impulsive and compulsive behavior by activating the mesolimbic dopamine system, in which dopaminergic inputs from the ventral tegmental area project to medium spiny neurons (MSN) of the nucleus accumbens (NAc) (Koob and Volkow, 2010). Furthermore, glutamatergic inputs to the NAc from the amygdala, frontal cortex, and hippocampus contribute to motivational action through the extrapyramidal motor system(Koob and Volkow, 2010). Subsequently, the NAc sends outputs to different nuclei of the ventral pallidum critical for processing and modulating substance reward signal(Koob and Volkow, 2010). The dorsal striatum (STR) is also hypothesized to be recruited during the development of compulsive substance-seeking(Koob and Volkow, 2010). Additionally, the dorsal striatum and prefrontal cortical regions(Goldstein and Volkow, 2011) regulate reward and addiction-related phenotypes. The findings emphasize the interplay of brain regions and the cellular components involved in substance use behavior.

Increasing evidence reveals strong genetic links to substance use risk(Pasman et al., 2018; Erzurumluoglu et al., 2019; Karlsson Linnér et al., 2019; Liu et al., 2019b) and SUD(Kendler and Prescott, 1998a, 1998b; Dick, 2016; Waaktaar et al., 2018). Genome-wide association studies

(GWAS) report that genetic risk for substance use shares underlying architecture with other neuropsychiatric disorders(Pasman et al., 2018; Liu et al., 2019b), of which risk variants tend to lie in non-coding and functional regions of the human genome(Jensen, 2016). These single nucleotide polymorphisms (SNPs) can disrupt transcription factor binding in cis-regulatory elements (CREs) with varying impact on gene regulation and downstream neural circuitry. Many CREs have tissue- and cell type-specific activity(Roadmap Epigenomics Consortium et al., 2015), suggesting that cell types and tissues underlying addiction may be uniquely targeted by genetic variants at these CREs. GWAS for nicotine-, alcohol-(Liu et al., 2019b), and cannabis-use traits(Pasman et al., 2018) have identified multiple confident risk loci and SNPs linked to addiction-associated phenotypes with brain-specificity, yet their effects on the CREs of specific brain regions and cell types involved in addiction pathophysiology are an open area of inquiry.

GWAS have found that SNP enrichment within functional non-coding regions contribute disproportionately to heritability of complex traits due to polygenicity(Finucane et al., 2015). Linkage disequilibrium (LD) of significant SNPs complicates the identification of causal variants contributing to genetic risk(Bush and Moore, 2012). The functional consequences of risk SNPs in CRE sequences cannot be reliably inferred from DNA sequences alone(Shlyueva et al., 2014). Recent developments in epigenomic assays(Buenrostro et al., 2013; Mo et al., 2015; Tak and Farnham, 2015) and machine learning(Ghandi et al., 2014; Zhou and Troyanskaya, 2015; Kelley et al., 2016, 2018; Lee, 2016) can predict cell types affected by addiction-associated genetic variation to propose cell type-specific hypotheses on the pathogenesis of addiction.

Here, we implement a framework that identifies regions and cell types that are affected by genetic risk variants for addiction-associated traits. We intersect these GWAS variants across human and mouse datasets from bulk tissue and cell type-specific open chromatin assays to

identify region- and cell type-specific CREs that may be impacted by genetic variation associated with addiction-related traits. We then apply machine learning models to predict open chromatin activity in key neuronal subtypes within reward circuits and refine our GWAS enrichments in these subtypes. Further, we apply these models to screen for putative causal SNPs within dense loci reported in GWAS for addiction-associated traits. This pipeline, to our knowledge, describes the first integrative analyses across species, regions and cell types to screen for candidate causal addiction-associated genetic risk variants in dense loci with numerous significant SNPs in LD.

RESULTS

Genetic risk for substance use traits is associated with the neuronal epigenomes of reward areas

Recent well-powered GWAS have characterized the genetic loci associated with seven addiction-associated traits, revealing several candidate loci encoding addiction genetic risk(Pasman et al., 2018; Karlsson Linnér et al., 2019; Liu et al., 2019b). These GWAS identify genetic variants associated with reward, risk tolerance, and various substance use behaviors to provide a means of studying genetic variation associated with addiction. We found that 72-98% of addiction-associated genetic variants map to noncoding intronic or intergenic regions of the genome **(Figure 1A)**. The proportion of intronic risk variants (47%-85%) overrepresented the proportion of intronic variants on the reference genotype panel (odds ratio, $OR_{AgeOfInit}$ =2.3, $OR_{Cannabis}$ = 2.3, $OR_{CigsPerDay}$ = 1.4, $OR_{DrinksPerWeek}$ = 1.6, $OR_{RiskyBehavior}$ = 1.4, $OR_{SmokCess}$ = 1.8, $OR_{SmokInit}$ =1.3, Fisher's Exact $P_{Bonferroni} < 8 \times 10^{-79}$). Furthermore, these seven traits have shared and distinct genetic architecture estimated using genetic correlation of risk alleles (r_g, **Supplemental Figure 1A**). Although common genetic variants are shared between addiction-associated traits on a genome-wide scale, the reported significant loci are often unique to a particular trait and are densely packed with SNPs in high LD (**Supplemental Figure 1B**).

We investigated whether genetic variants of addiction-associated GWAS cluster at putative cis-regulatory elements (CREs) of the brain using a partitioned heritability linkage disequilibrium score (LDSC) regression approach(Bulik-Sullivan et al., 2015b; Finucane et al., 2018) on open chromatin regions (OCRs) of sorted neuronal (NeuN+) and glial (NeuN-) nuclei across 14 brain regions(Fullard et al., 2018) **(Figure 1B)**. We found that genetic variants associated with having ever regularly smoked (`SmokingInitiation`), being a former versus current smoker

(SmokingCessation), the number of alcoholic drinks per week (DrinksPerWeek), and lifetime cannabis use (Cannabis) significantly enriched in NeuN+ OCRs of brain regions known and speculated to contribute to reward and addiction(Volkow and Morales, 2015) (FDR < 0.05). In particular, we found that genetic variants associated with SmokingInitiation and Cannabis shared enrichment in NeuN+ prefrontal cortical OCRs (from orbitofrontal cortex and dorsolateral prefrontal cortex) while those associated with SmokingCessation and DrinksPerWeek shared enrichment in NeuN+ striatal OCRs (both putamen and NAc). The enrichments of NeuN+ OCRs indicate that genetic variation in epigenomes of neuronal populations from frontal cortex and striatum contribute to addiction liability. The difference in NeuN+ enrichments between regions across addiction-associated traits can likely be explained by the difference in proportions of neuronal subtypes of each area, so we sought to dissect the different neuronal subtypes contributing to these enrichments.

Broad marker-gene based labeling approaches, such as using NeuN to label neurons, do not capture the rich diversity of neuronal subtypes; bulk NeuN+ open chromatin signal represents an average signal from heterogeneous neuronal subtypes, each with distinct epigenomic landscapes, gene regulation, network connectivity. Hence, NeuN-labeled open chromatin profiles likely do not capture OCRs unique to less populous neuronal subtypes. The difference in proportions of neuronal subtypes between brain regions may also contribute to brain region-specific NeuN+ OCR enrichment for GWAS variants of addiction-associated traits. We therefore applied LDSC regression GWAS enrichment on open chromatin profiles from human postmortem occipital cortex cell types via single-cell transposase hypersensitivity sequencing (scTHS-seq) (Lake et al., 2018) **(Figure 1C)**. We found that addiction-associated genetic variants largely enriched in both excitatory and inhibitory neuronal OCRs. We found enrichment of genetic

variants associated with age of smoking initiation (AgeOfInitiation) and SmokingCessation in OCRs of cortical excitatory neurons. We found no enrichment of genetic variants associated with average number of cigarettes smoked per day (CigarettesPerDay) for OCRs of occipital cortex cell types. Genetic variants associated with SmokingInitiation, which enriched in astrocyte, endothelial, inhibitory, and oligodendrocyte precursor cell OCRs, shared enrichment in NeuN- OCRs of mediodorsal thalamus **(Figure 1B)**. Interestingly, genetic variants associated with SmokingCessation, which had enriched for striatal NeuN+ OCRs, enriched only for OCRs of cortical excitatory neurons and not cortical inhibitory neurons. Sorted bulk ATAC-seq only showed enrichment of SmokingCessation associated genetic variants in OCRs of NeuN+ striatal regions, which are largely composed of inhibitory MSNs. Single-cell epigenomics of human postmortem brain can further dissect the genetic risk for substance-use traits into neuronal subtypes that otherwise would not be parsed with bulk tissue assays.

We confirmed that our pipeline for LDSC regression on NeuN-sorted OCRs from 14 brain regions is able to reproduce the GWAS enrichments published by Fullard *et al.* While our approach uses OCRs from reproducible ATAC-seq peaks rather than differentially accessible peaks, we found consistent enrichments of genetic variants associated with schizophrenia risk (Schizophrenia), highest level of educational attainment (EduAttain), and habitual sleep duration (SleepDuration) **(Supplemental Figure 2B)**. We did not find enrichment in brain OCRs of genetic variants identified in several low-powered GWAS (cocaine dependence (CocaineDep)(Cabana-Domínguez et al., 2019), opioid dependence (OpioidDep) (Cheng et al., 2018), and obsessive-compulsive disorder (OCD)(International Obsessive Compulsive Disorder Foundation Genetics Collaborative (IOCDF-GC) and OCD Collaborative Genetics

Association Studies (OCGAS), 2018), each of which had included fewer than 5000 individuals with the trait **(Supplemental Figure 2A)**. In addition, we found no enrichments in brain OCR for several well-powered studies of traits related to addiction behaviors, multi-site chronic pain (`ChronicPain`)(Johnston et al., 2019) and cups of coffee per day (`CoffeePerDay`)(Coffee and Caffeine Genetics Consortium et al., 2015) and anthropometric traits coronary artery disease (`CAD`) (Howson et al., 2017), bone mineral density (`BMD`) (Kemp et al., 2017), and lean body mass (`LBM`) (Zillikens et al., 2017) **(Supplemental Figure 2B, C)**. Lastly, we validated that human OCRs from non-brain tissues would not enrich for risk variants associated with brain traits. We gathered publicly available OCRs from stomach ATAC-seq, adipocyte ATAC-seq, preadipocyte ATAC-seq, liver DNase-seq, and lung DNase-seq profiles(ENCODE Project Consortium, 2012; Thurman et al., 2012; Davis et al., 2018; Cannon et al., 2019) **(Supplemental Figure 4D)** and performed LDSC regression on the total 18 GWAS from above. To our expectation, we did not find enrichments of stomach, liver, or lung OCRs for genetic variants associated with brain-related traits. We did find enrichment of `BMD` in lung OCRs, a connection previously recognized(Lee et al., 2016; Kim et al., 2019; Zeng et al., 2019). The secondary GWAS enrichments in other traits and foregrounds demonstrate two trends: a GWAS trait would enrich if the GWAS was properly powered to detect genetic risk variants, and the foreground regions are from cell types or tissue of that trait's potential etiological origin.

Mouse-human conserved cell type-specific open chromatin enrich for addiction risk loci

In order to resolve the different neuronal subtypes that comprise the addiction-associated enrichments in Fullard *et al.* and Lake *et al.* OCRs **(Figure 1, Supplemental Figure 2)**, we performed targeted epigenomics in mouse to isolate various neuronal subtypes from frontal cortex

(CTX), caudoputamen (CPU), and the nucleus accumbens (NAc), which are key brain regions of the reward circuit. We isolated cell type-specific nuclei for ATAC-seq using a modified version of the INTACT approach(Mo et al., 2015), which we call *cre*-specific nuclei anchored independent labeling (cSNAIL). cSNAIL-INTACT uses the AAV-PHP.eB virus to isolate nuclei marked by *Pvalb*, *Sst*, *Drd1*, and *Adora2a cre*-lines without crossing with a *Sun1-Gfp* transgenic mouse **(Figure 2A)**. We show that cell type-targeting provided markedly distinct genome-wide ATAC-seq profiles compared to bulk tissue ATAC-seq alone (**Supplemental Figure 3A**). cSNAIL ATAC-seq specifically captured nuclei with increased accessibility around the marker gene that was driving *Cre* recombinase expression (**Supplemental Figure 3B**). Accessibility around cSNAIL ATAC-seq transcription start sites (TSS) strongly correlated with matched pseudobulk gene expression in the same cell type and tissue (**Methods**, both Pearson and Spearman correlation $P_{bonf} < 2 \times 10^{-16}$, **Supplemental Figure 3C,D**). We applied the HALPER approach(Zhang et al., 2020) to reliably map ~70% of mouse OCRs to their human orthologs in hg38 **(Methods)** to run LDSC regression GWAS enrichments.

Our GWAS enrichments of human orthologs from mouse OCRs of various neuronal subtypes and bulk tissue **(Figure 2B)** show that genetic variants associated with `SmokingInitiation` and `Cannabis` shared enrichment in human orthologs of mouse cortical PV and EXC neuron OCRs from both Mo *et al.* and this study (FDR < 0.05). Cannabis associated genetic variants further enriched in CTX bulk tissue OCRs, which could be attributed to signal from cortical EXC and PV neuron populations. Cortical PV neuron OCRs further enriched with genetic variants associated with `DrinksPerWeek`. `SmokingCessation` associated genetic variants distinctly enriched in cortical VIP neuron OCRs.

Within cell types from CPU and NAc, we found enrichment of genetic variants associated with all measured addiction-associated traits in CPU and NAc D2 MSN OCRs. Genetic variants associated with all measured traits excluding `SmokingInitiation` and `RiskyBehavior` all enriched in CPU and NAc D1 MSN OCRs. CPU D1 MSN OCRs were enriched with genetic variants associated with all measured traits excluding `RiskyBehavior`. We found that CPU bulk tissue OCRs were enriched with genetic variants associated with all measured addiction-associated traits excluding `AgeOfInitiation` and `RiskyBehavior`. Distinctly, CPU PV+ and SST+ neuron OCRs enriched with genetic variants associated with `Cannabis`.

Corresponding to our analysis of human brain OCRs, we also confirmed the specificity of mouse-human orthologous CRE enrichments for genetic variants of addiction-related, brain-related, and non-brain related traits **(Supplemental Figure 4)**. We found enrichments of genetic variants associated with `ChronicPain` in cortical PV neuron OCRs from both Mo *et al.* and this study **(Supplemental Figure 4A).** Within striatal cell types, we found that CPU D2 and NAc D1 MSN OCRs were enriched for genetic variants associated with `ChronicPain`. In contrast, CPU D1 and NAc D2 MSN OCRs were enriched for genetic variants associated with `OpioidDep`. Genetic variants associated with `OpioidDep` also enriched in CPU D1 MSN and CPU PV OCRs. `Schizophrenia`, `EduAttain`, and `SleepDuration` associated genetic variants all enriched in OCRs of all measured cell types **(Supplemental Figure 4B)**. None of these human orthologs of mouse neuronal OCRs enriched for genetic variants associated with non-brain-related traits `BMD`, `CAD`, and `LBM` **(Supplemental Figure 4C)**. We validated that our approach to map OCRs from mouse to human did not bias enrichment to brain traits by performing GWAS enrichment on OCRs from mouse non-brain tissues (kidney, liver, and lung) **(Supplemental Figure 4D)**. As expected, we did not find an enrichment for genetic variants associated with a

brain-related trait. We did find that human orthologs of lung OCRs enrich for BMD, which concords with the enrichment of human lung OCRs.

Machine learning models of mouse cell type-specific CRE activity refine human NeuN+ OCRs for GWAS enrichment

Assays such as ATAC-seq capture the open chromatin genomic regions that can be occupied by DNA-binding regulatory proteins. DNA-binding proteins and their cofactors regulate gene expression, often in response to external stimuli; therefore, the DNA sequences underlying OCRs reveal the complex combinations of DNA-binding protein motif, i.e. the "*cis*-regulatory grammar," that is being read by regulatory proteins to define the cell's epigenetic state. We hypothesized that conservation of OCRs between mouse and humans must also rely on a conserved regulatory grammar to maintain the similar cell identity between human and mouse (Chen et al., 2018). The concordant pattern of enrichment for addiction associated genetic variants in human and mouse-human orthologous OCRs suggested that risk variants may affect the regulatory grammar of cell types conserved in mouse. We therefore trained a collection of convolutional neural network (CNN) machine learning (ML) models to learn the regulatory grammar for cortical excitatory (EXC) neurons, striatal D1 MSNs, and striatal D2 MSNs (Zhou and Troyanskaya, 2015; Kelley et al., 2016, 2018; Chen et al., 2018). For each set of reproducible OCRs from mouse INTACT and cSNAIL group, we trained 5-fold cross-validated models to predict the reproducible peaks from ten times the number of GC-matched negative sequences **(Methods)**. Our models made confident predictions on held-out test sequences as reported by accuracy, F1-score, and areas under the receiver-operator characteristic and precision-recall curves **(Supplemental Figure 5A)**.

We reasoned that NeuN+ OCR signal that is comprised of several neuronal subtypes that can be parsed into component cell types by ML models trained to predict OCR activity in those cell types. To discern whether NeuN+ OCR enrichments in addiction-associated genetic variants come from the same cell types that we see in **Figure 3**, we used the ML models to predict whether cortical or striatal NeuN+ OCRs have activity in cortical EXC or striatal D1 and D2 cells, respectively **(Figure 3A)**. We did not conduct these analyses for PV neurons because they comprise a much lower percentage of cortical and striatal neurons than the other neuron types. We ran LDSC regression (Finucane et al., 2018) GWAS enrichments on the sets of NeuN+ OCRs predicted to be specific to cortical EXC, striatal D1, and striatal D2 neurons. Genetic variants associated with `SmokingInitiation`, which initially enriched in OCRs of various NeuN+ frontal cortical areas **(Figure 1B)**, enriched in NeuN+ OCRs predicted to be active in EXC neurons **(Figure 3B)**. Genetic variants associated with `Cannabis`, which enriched in NeuN+ cortical OCRs **(Figure 1B)**, also enriched in NeuN+ OCRs predicted to be active in EXC neurons. The enrichments of excitatory cortical cell type-specific OCRs for `SmokingInitiation` and `Cannabis` associated genetic variants agree with the results from the Fullard *et al*. and Lake *et al*. human datasets **(Figure 1B, C)**. Genetic variants associated with `SmokingCessation` and `DrinksPerWeek`, which enriched in PUT and NAc NeuN+ OCRs **(Figure 1B)**, shared enrichment in OCRs predicted active in both D1 and D2 MSNs of both PUT and NAc. The framework that we outline in **Figure 3A** refines addiction genetic risk signal to neuronal subtypes, maintains the brain region context of the source NeuN+ OCR, and can be applied to CREs from any tissue, cell type combination for which bulk tissue open chromatin exists in human and open chromatin from that cell type exists in another vertebrate(Chen et al., 2018; Minnoye et al., 2020).

Machine learning models predict allele-specific activity of addiction-associated GWAS SNPs in neuronal subtypes

Lastly, we applied our ML models to screen addiction-associated genetic variants for predicted functional activity in EXC, D1, and D2 neuronal subtypes. These ML-based approaches have been demonstrated to fine-map dense risk loci and select candidate causal genetic variants (Alipanahi et al., 2015; Zhou and Troyanskaya, 2015; Kelley et al., 2016, 2018), yet none have been applied in the context of addiction-associated genetic risk or in the cell types that we have assayed. We collected 14,790 SNPs across the seven addiction-associated GWAS and filtered down to 170 SNPs that are in NeuN+ OCRs and predicted to be causal with statistical fine-mapping **(Methods)**. We demonstrated that our cortical and striatal ML models produce scores near 0 (no predicted open chromatin activity in this cell type) for SNPs not in any OCRs, low scores for SNPs in NeuN- OCRs, and significantly larger scores (larger predicted open chromatin in this cell type) for SNPs in NeuN+ OCRs ($P_{Bonferroni} < 0.05$, **Figure 4A)**. Using these models and the 170 filtered SNPs, we prioritized 26 unique SNPs spanning 16 loci with predicted functional consequence on gene regulation **(Supplemental Figure 5B, Methods)**. One such SNP, rs7604640, lies in NeuN+ open chromatin specific to striatum ~46kb upstream of the *SIX3* locus on chromosome 2. rs7604640 overlaps human orthologs of mouse OCRs in only D1 and D2 neurons and had predicted open chromatin activity in both D1 and D2 neurons but not in EXC neurons **(Figure 4B)**. rs7604640 is one of many off-lead SNPs identified in the `SmokingInitiation` GWAS ($P_{GWAS} = 3.04 \times 10^{-12}$) and is in LD with the lead SNP rs163522 ($R^2 = 0.856$). Furthermore, this SNP is a known *cis*-eQTL for the antisense *SIX3-AS1* gene in striatal regions from the Genotype-Tissue Expression (GTEX) project (GTEx Consortium, 2013, 2015; Melé et al., 2015; GTEx Consortium et al., 2017). Anti-sense gene expression is one mechanism of regulating their sense

gene(Pelechano and Steinmetz, 2013; Barman et al., 2019), and deletion of the gene *SIX3* has been shown to inhibit development of D2 medium spiny neurons (Xu et al., 2018). Altogether, this evidence formulates the hypothesis that common genetic variant rs7604640 has D1 and D2 MSN-specific open chromatin activity in a mouse-human conserved putative CRE regulating the MSN regulator *SIX3*.

We found a number of other SNP candidates that may be putative causal SNPs with cell type-specific activity in addiction-associated traits **(Supplemental Figure 6)**. For example, SNPs rs11191352 ($P_{SmokingInitiation}$=2.12 x 10^{-7}) and rs9844736 ($P_{RiskyBehavior}$= 3.04 x 10^{-7}, $P_{SmokingInitiation}$=3.58 x 10^{-7}) are both *cis*-eQTL for nearby genes in GTEx striatal regions **(Supplemental Figure 6A,B)**. Curiously, SNPs such as rs7604640, rs10742814, and rs11191352 had predicted cell type-specific activity in only MSNs **(Figure 4B, Supplemental Figure 6A,B)**, while the SNP rs9844736 had predicted activity in mouse-human orthologous CREs from all three cell types **(Supplemental Figure 6D)**. SNPs rs6870603 ($P_{SmokingInitiation}$=1.04 x 10^{-8}) and rs7712167 ($P_{SmokingInitiation}$=8.79 x 10^{-9}), which are 317bp apart, were predicted to alter only EXC open chromatin activity and lie in a strong cortical-specific NeuN+ OCR. The complete summary of prediction scores and annotations of GTEX eQTL membership for each SNP can be found in **Supplemental Table 1**.

DISCUSSION

In this study, we demonstrate the first analyses integrating cell type OCRs across human and mouse brain epigenomics using ML models to select candidate addiction-associated SNPs acting at putative cell type-specific CREs. We trained ML models to predict cell type-specific activity of OCRs and used the models to predict whether addiction-associated genetic variants in risk loci impact putative CRE function. Our findings link the genetic heritability of addiction-associated behaviors to the OCR profiles of neuronal subtypes and brain regions and present specific hypotheses describing how genetic variants may impact gene regulation in addiction-associated behaviors. These analyses in conjunction suggest that genetic variation-associated nicotine, alcohol, and cannabis use behaviors may impact putative CREs in different combinations of excitatory (EXC), D1, and D2 neuronal subtypes. These findings provide a foundation for future investigations into the cell type-specific genetic mechanisms underlying addiction-related traits. More broadly, our cross-species integrative computational framework leverages high-resolution cell-type targeted epigenomics in model organisms to interpret the genetic risk variants of complex traits in humans.

We initially found that addiction-associated genetic variants were enriched in human NeuN+ OCRs of the prefrontal cortex and striatum, known areas involved in addiction and reward circuitry(Volkow et al., 2013; Koob and Volkow, 2016) **(Figure 5A)**. Genetic variants associated with `SmokingInitiation` and `Cannabis`, initiating behaviors of substance use, were enriched in NeuN+ OCRs of prefrontal areas including DLPFC, VLPFC, and OFC **(Figure 1B)**. These OCRs were predicted to be active in cortical excitatory neurons of these brain regions **(Figure 3B)**. Addiction-associated genetic variants that enrich in OCRs of cortical excitatory neurons in these areas may reduce corticostriatal activation from prefrontal cortex to inhibit

behaviors predisposing the initiation of substance use(Koob and Volkow, 2010, 2016; Volkow et al., 2013; Volkow and Morales, 2015). These genetic variants may contribute to reduced prefrontal self-control reward, leading to behaviors observed in addiction such as impulsivity, reduced satiety, and enhanced motivation to procure drugs(Volkow et al., 2013; Volkow and Morales, 2015). In addition, we found enrichment of striatal NeuN+ OCRs for genetic variants associated with `SmokingCessation` and `DrinksPerWeek` **(Figure 1B)**. In **Figure 3B**, we showed that these genetic variants are predicted to affect open chromatin in both D1 and D2 MSNs, which are coordinators of mesocorticostriatal dopamine systems(Koob and Volkow, 2010, 2016; Volkow et al., 2013). Genetic variants affecting open chromatin in these MSN subtypes may predispose individuals to increased alcohol use (`DrinksPerWeek`) or decreased nicotine use (`SmokingCessation`), perhaps driving the neuroplastic changes in D1 and D2 MSNs observed in human and rodent drug dependence studies(Volkow et al., 1996, 1997, 2003; Wang et al., 1997; Fehr et al., 2008; Cheng et al., 2017; Wilar et al., 2019). While drug addiction has been attributed to various areas of the reward circuit, our investigations into heritable genetic risk for addiction-associated traits unravel how regulatory DNA sequence variation in OCRs of projection neurons in implicated areas link genetic risk to neural circuits to behavior.

Since cell types in the occipital cortex are not clearly defined for their role in the reward circuit, we conducted ATAC-seq of projection and interneuron subtypes in mouse brain, mapped OCRs to human orthologs, and analyzed GWAS enrichment of addiction-associated traits. By leveraging ortholog mapping tools, we retained high-quality cell type-specific measurements within relevant brain regions of the reward circuit, enabling analysis of cell populations from brain regions where we lack primary human open chromatin profiles. Across these brain regions, we found remarkably concordant enrichments of cell type OCRs between mouse and human profiles

as well as shared enrichments between traits **(Figure 5B)**. Genetic variants associated with both `SmokingInitiation` and `Cannabis` enriched in mouse-human orthologous OCRs of cortical EXC and PV neurons **(Figure 3B)**, concordant with enrichments in human cortical NeuN+ OCRs **(Figure 1B)**, which were predicted to include EXC neurons **(Figure 4B)**. Genetic variants from these two traits showed replicable enrichment in human EXC and IN neuron OCRs via sc-THS-seq of occipital cortex **(Figure 1C**), providing strong evidence that genetic variation in cortical excitatory and inhibitory neuron OCRs confers susceptibility to nicotine and cannabis use behaviors. Within striatal regions, D1 and D2 MSN mouse-human orthologous OCRs enriched for genetic variants of all measured addiction-associated traits **(Figure 2B)**, with strongest concordance in human OCRs for genetic variants associated with `SmokingCessation` and `DrinksPerWeek` **(Figure 3B, Figure 5B)**. The enrichments in conserved OCRs of MSN subtypes in the dorsal striatum and nucleus accumbens unsurprisingly emphasize known roles of MSNs of both areas to drive and maintain addiction behaviors(Ferguson et al., 2011; Ji et al., 2017).

In an orthogonal approach to mapping mouse-human orthologous OCRs, we leveraged machine learning models to learn the regulatory grammar of neuronal subtypes characterized in mouse and refine human NeuN+ OCRs to the major neuronal subtypes of cortex and striatum for GWAS enrichment. Refinement of NeuN+ OCRs revealed that addiction-associated traits enriched for two clusters of cell types and brain regions. The first group, which displays concordant cortical excitatory enrichments between human and mouse, consists of `SmokingInitiation` and `Cannabis` **(Figure 3B)**, and the second group, which displays concordant D1 and D2 MSN enrichments, consists of `SmokingCessation` and `DrinksPerWeek`. A draw-back of assigning human NeuN+ OCR membership to individual cell types lies in the considerably low

representation of interneurons in both cortical and striatal neuron populations - as low as 12% in neocortex(Beaulieu, 1993; Lefort et al., 2009) and ~5% in striatum(Tepper and Koós, 2017; Krienen et al., 2019). NeuN+ open chromatin profiles alone do not always capture OCRs unique to rare interneurons, some of which had OCRs identified by human single-cell assays and mouse-human orthologs enriched for addiction GWAS variants **(Figure 1C, Figure 2B)**. As a result, we did not train ML models for PV, SST, or VIP interneurons. However, the striking enrichments of OCRs from certain interneuron populations for addiction GWAS variants begin to demonstrate these populations' roles in the addiction neural circuits(Bracci et al., 2002; Lansink et al., 2010; Wiltschko et al., 2010; Ribeiro et al., 2018; Jiang et al., 2019; Lee et al., 2020; Schall et al., 2020).

The overall concordance of enrichments across human and mouse-human orthologous OCRs suggests a conserved regulatory grammar between mouse and human CREs. Correspondence in the neural circuitry has been well-appreciated between human studies and rodent models of addiction(Berke and Hyman, 2000; Koob and Volkow, 2016; Farrell et al., 2018), and our study further demonstrates that mouse-human conserved OCRs may explain considerable heritability of addiction-associated traits. This makes animal models suitable not only for studying the neural circuits of addiction but also cell-type-specific gene-regulatory mechanisms of addiction.

We used several selection criteria along with ML models to predict the functional impact of genetic variants that may be agents in addiction-associated traits **(Figure 5, Supplemental Figure 5, Supplemental Table 1)**. The fine-mapping pipeline described effectively narrows down a set of 14,790 SNPs to a putatively functional set of 26 candidates that can be experimentally tested to determine which brain regions and neuronal subtypes they would have function in. The candidate functional SNPs that our models prioritize demonstrate how a candidate SNP within a

439 locus, such as rs7604640 **(Figure 4B)**, might act in different combinations of neuronal subtypes
440 and brain regions. This pleiotropy adds complexity to discerning which neuronal subtypes have
441 altered gene regulation in addiction-associated traits. Our approach often reported only one or two
442 candidates per loci, reflecting the idea that many SNPs in the same loci are significantly associated
443 with addiction due to LD with the causal SNP and may not influence addiction-associated genetic
444 predisposition. The candidate SNPs that overlap mouse-human orthologs from the same predicted
445 cell type raise the idea that altering the conserved regulatory DNA sequence may be a mechanism
446 of cell type-specific gene regulatory tuning in a population or even across species(Gjoneska et al.,
447 2015).

448 Our study depends solely on assays of open chromatin as a proxy for putative CREs.
449 Epigenetic assays for chromatin conformation, histone modifications, and methylation would
450 further inform how putative CREs regulate nearby gene expression. Furthermore, our predictions
451 of SNP impact on putative CREs and genes remain to be experimentally validated. While eQTL
452 studies do not control for inflated associations due to LD and report gene expression differences
453 from bulk tissue, we do note that our approach prioritizes several SNPs known to be *cis*-eQTLs in
454 relevant brain regions, which indirectly affirms our framework's ability to select SNPs with
455 functional impacts on gene regulation. In order to validate our predictions, it will be necessary to
456 further investigate candidate genetic variants such as rs7604640 **(Figure 4B)** in future studies
457 using massively parallel reporter assays(Tewhey et al., 2016) or self-transcribing active regulatory
458 region sequencing(Vockley et al., 2015; Kalita et al., 2018) that can measure regulatory activity
459 differences between risk and non-risk alleles. The candidate SNPs we identified provide possible
460 mechanisms linking differences in genetic make-up with the genes, cell types, and brain regions
461 that could influence addiction and substance use behaviors **(Figure 4)**.

MATERIALS & METHODS

ATAC-seq data processing pipeline:

We processed raw FASTQ files of ATAC-seq experiments with the official ENCODE ATAC-seq pipeline (Landt et al., 2012) accessed by https://github.com/ENCODE-DCC/atac-seq-pipeline. We ran this pipeline using the `mm10` genome assembly for mouse and the `hg38` genome for human with the following settings: `smooth_win = 150`, `multimapping = 0`, `idr_thresh = 0.1`, `cap_num_peak = 300,000`, `keep_irregular_chr_in_bfilt_peak = true`. We grouped biological replicates when processing data to obtain individual de-duplicated, filtered bam files and reproducible (IDR) peaks for each condition. Unless otherwise stated, we used the optimal reproducible set of peaks for downstream analyses. We removed samples that had low periodicity indicated by ENCODE quality control metrics and reprocessed the remaining replicates with the pipeline.

Publicly available datasets

Fullard *et al.* NeuN-sorted ATAC-seq of human postmortem brain (Fullard et al., 2018): We identified OCRs overlapping addiction-related variants through analysis of human postmortem brain ATAC-seq in which cells were sorted into NeuN-positive and NeuN-negative groups via fluorescence activated nuclei sorting (FANS); the brain regions we used were dorsolateral prefrontal cortex (DLPFC), orbitofrontal cortex (OFC), ventrolateral prefrontal cortex (VLPFC), anterior cingulate cortex (ACC), superior temporal gyrus (STC), inferior temporal gyrus (ITC), primary motor cortex (PMC), insula (INS), primary visual cortex (PVC), amygdala (AMY), hippocampus (HIP), mediodorsal thalamus (MDT), nucleus accumbens (NAc), and putamen (PUT). We downloaded data from the Sequence Read Archive (SRA) through Gene Expression Omnibus (GEO) accession #GSE96949. We separated samples by cell type and reprocessed them

with the ENCODE pipeline as detailed above, aligning reads to `hg38`. We used the "optimal reproducible peaks" for each cell type and brain region as foregrounds in GWAS LDSC enrichment with the Honeybadger2 OCR set as the background set (see LDSC Regression GWAS Enrichment Backgrounds).

Lake et al. human occipital cortex scTHS-seq (Lake et al., 2018): We downloaded BED-formatted cell type-specific differential OCRs from occipital cortex scTHS-seq of excitatory neurons (EXC), inhibitory neurons (IN), astrocytes (AST), endothelial cells (END), oligodendrocyte precursor cells (OPC), oligodendrocytes (OLI), and microglia (MIC) from the GEO subseries #GSE97887. We used the `hg38` OCR coordinates as foregrounds in LDSC regression GWAS enrichment with the Honeybadger2 OCR set as the background set (LDSC regression GWAS Enrichment Backgrounds).

Mo *et al.* mouse INTACT-sorted nuclei ATAC-seq (Mo et al., 2015): We downloaded FASTQ files of *R26-CAG-LSL-Sun1-sfGFP-Myc* transgenic mouse lines for cell type-specific ATAC-seq performed using the INTACT method from the accession #GSE63137. *Mo et al.* isolated INTACT-enriched nuclei from three cell types: excitatory neurons (EXC, *Camk2a-cre*), vasoactive intestinal peptide neurons (VIP, *Vip-cre*), and parvalbumin neurons (PV, *Pvalb-cre*). We reprocessed the data with the Kundaje Lab open chromatin pipeline using the mm10 genome (`https://github.com/kundajelab/atac_dnase_pipelines`). We mapped reproducible mouse ATAC-seq peaks for each cell type to `hg38` using halLiftover with the 12-mammals Cactus alignment (Paten et al., 2011; Hickey et al., 2013) followed by HALPER (Zhang et al., 2020) (Mapping mouse OCR orthologs) to produce a foreground set of orthologous human sequences for LDSC regression GWAS enrichment (Finucane et al., 2018). We mapped the ENCODE `mm10` DNaseI-hypersensitive peak set(Yue et al., 2014) to `hg38` (Mapping mouse OCR

508 orthologs) and used successfully mapped hg38 orthologs of mm10 OCRs a background set for
509 mouse foreground enrichments. Furthermore, we used this dataset to evaluate differential
510 accessibility in cSNAIL-INTACT PV and PV-negative ATAC-seq samples and develop machine
511 learning models of cell type-specific open chromatin (see Methods below).
512 Human negative control foregrounds (ENCODE Project Consortium, 2012; Thurman et al., 2012;
513 Davis et al., 2018; Cannon et al., 2019): We downloaded raw ATAC-seq profiles of human adult
514 female and male stomach ATAC-seq generated by Snyder *et al*. (ENCSR337UIU,
515 ENCSR851SBY, respectively), female human embryonic liver DNase-seq generated by
516 Stamatoyannopoulos *et al*. (ENCSR562FNN), and human embryonic lung DNase-seq generated
517 by Stamatoyannopoulos *et al*. (ENCSR582IPV) from
518 `https://www.encodeproject.org/`. We processed these files using the ENCODE
519 pipeline as detailed above to obtain optimal reproducible `hg38` peaks. We also downloaded BED
520 files of human adipocyte and preadipocyte ATAC-seq profiles generated by Cannon *et al*. from
521 GEO accession number #GSE110734. We mapped these BED coordinates from `hg19` to `hg38`
522 using liftOver to define negative control foregrounds for human LDSC regression GWAS
523 enrichment. We merged the human negative control foregrounds and Fullard *et al.* foregrounds
524 with the Honeybadger2 OCR set to define the background for human negative control foreground
525 enrichments.
526 Human-orthologous negative control foregrounds (Liu et al., 2019a): We also downloaded raw
527 ATAC-seq data profiled in female mouse kidney, female mouse liver, and male mouse lung
528 generated by Liu *et al.* from SRA accession #SRP167062 to define human-orthologous negative
529 control foregrounds. We processed these files using the ENCODE pipeline as detailed above to
530 get optimal reproducible peaks. We mapped optimal reproducible peaks from `mm10` to `hg38` using

halLiftover with the 12-mammals Cactus alignment followed by HALPER (Mapping mouse OCR orthologs) to define negative control foregrounds for human-orthologous LDSC GWAS enrichments. We merged all human orthologous foregrounds with the human orthologs of the ENCODE `mm10` DNaseI-hypersensitive peak set to define a background for human-orthologous LDSC GWAS enrichments.

Mapping mouse open chromatin region (OCR) orthologs

We employed halLiftover (Hickey et al., 2013) with the 12-mammals Cactus alignment (Paten et al., 2011) followed by HALPER (`https://github.com/pfenninglab/halLiftover-postprocessing`)(Zhang et al., 2020) to map `mm10` mouse reproducible OCRs to `hg38` human orthologs in order to perform LDSC regression GWAS enrichment. The Cactus multiple sequence alignment file (Paten et al., 2011) has 12 genomes, including `mm10` and `hg38`, aligned in a reference-free manner, allowing us to leverage multi-species alignments to confidently identify orthologous regions across species. halLiftover uses a Cactus-format multiple species alignment to map BED coordinates of a query species to orthologous coordinates of a target species, and HALPER constructs contiguous orthologs from the outputs of halLiftover (Zhang et al., 2020). We ran the `orthologFind.py` function from HALPER on the outputs of halLiftover using the following parameters: `-max_frac 5.0 -min_frac 0.05 -protect_dist 5 -narrowPeak -mult_keepone`. In general, 70% of mouse brain ATAC-seq reproducible peaks were able to be mapped to confident human orthologs. To map the ENCODE `mm10` mouse DHS background, which does not contain summit information, to `hg38` we used the mouse coordinates of position with the most species aligned in a region to define the summit. Only for the `mm10` mouse DHS background set, for which a significant proportion of regions could not be confidently mapped to

554 hg38, we flanked the original assembly coordinates by 300 bp to increase OCR mapping from
555 54% to 64%.

556 **LDSC Regression GWAS Enrichment Backgrounds:**

557 We found that LDSC regression GWAS enrichment analysis is sensitive to the selected
558 background set of matched regions. To construct appropriate background sets for each GWAS
559 enrichment, we used the ENCODE and RoadMap Honeybadger2(Roadmap Epigenomics
560 Consortium et al., 2015) and Mouse DHS peak sets for the respective human and mouse-based
561 open chromatin GWAS enrichment. The Honeybadger2 set, downloaded from
562 https://personal.broadinstitute.org/meuleman/reg2map/, consists of
563 DNaseI-hypersensitive OCRs across 53 epigenomes consisting of promoter, enhancer, and dyadic
564 regions. Honeybadger2 is an appropriate epigenetic reference for enrichment of cell type-specific
565 open chromatin from various foregrounds such as the Fullard *et al.* and Lake *et al*. Honeybadger2
566 regions allow the LDSC algorithm to properly account for the heritability from OCRs of a
567 particular cell type or regions rather than because they tend to be more conserved, are enriched for
568 ubiquitously active transcription factor motifs, or other factors distinguishing open chromatin from
569 heterochromatin. The human orthologs of the ENCODE Mouse DHS peak set, downloaded
570 through the ENCODE ATAC-seq pipeline at
571 http://mitra.stanford.edu/kundaje/genome_data/mm10/ataqc/mm10_un
572 iv_dhs_ucsc.bed.gz, is a set of peaks combined from mouse DNaseI-hypersensitivity
573 OCRs from ENCODE and provides a background for human orthologs of mouse OCRs. The mm10
574 mouse DHS regions were mapped to hg38 as described in **Mapping mouse OCR orthologs**. For
575 each respective foreground-background pairing, the foreground regions were merged with the
576 background reference to ensure the background always contained the foreground set. The mouse

background was used to calculate the significance of the relationship between mouse OCRs and GWAS for addiction-associated traits to control for a possible association between the degree to which a region is conserved and its likelihood in influencing the predisposition to an addiction-associated trait.

GWAS enrichment with partitioned LD score regression analysis

We computed the partitioned heritability of CREs for GWAS variants using the LDSC regression pipeline for cell type-specific enrichment as outlined in `https://github.com/bulik/ldsc/wiki/Cell-type-specific-analyses`(Bulik-Sullivan et al., 2015b). We downloaded the GWAS summary statistics files and processed them with the LDSC `munge_sumstats` function to filter rare or poorly imputed SNPs with default parameters. We munged the summary statistics files for HapMap3 SNPs excluding the MHC regions downloaded at `http://ldsc.broadinstitute.org/static/media/w_hm3.noMHC.snplist.zip`. We inspected GWAS file to ensure the effect allele, non-effect allele, sample size, p-value, and signed summary statistic for each SNP in each GWAS were included and appropriate for LDSC. The addiction-associated GWAS measure genetic predisposition for age of smoking initiation (`AgeofInitiation`)(Liu et al., 2019b), heaviness of smoking (`CigarettesPerDay`)(Liu et al., 2019b), having ever regularly smoked (`SmokingInitiation`)(Liu et al., 2019b), current versus former smokers (`SmokingCessation`)(Liu et al., 2019b) , alcoholic drinks per week (`DrinksPerWeek`)(Liu et al., 2019b), cannabis consumption (`Cannabis`)(Pasman et al., 2018), and risk tolerance (`RiskyBehavior`)(Karlsson Linnér et al., 2019). GWAS traits related to addiction include multisite chronic pain (`ChronicPain`)(Johnston et al., 2019) and number of coffee cups drank

per data (CoffeePerDay)(Coffee and Caffeine Genetics Consortium et al., 2015). Other addiction-related traits come from underpowered GWAS including opioid dependence (OpioidDep)(Cheng et al., 2018) , cocaine dependence (CocaineDep)(Cabana-Domínguez et al., 2019), and diagnosis of obsessive-compulsive disorder (OCD)(International Obsessive Compulsive Disorder Foundation Genetics Collaborative (IOCDF-GC) and OCD Collaborative Genetics Association Studies (OCGAS), 2018). GWAS from strong brain-related traits used are schizophrenia risk (Schizophrenia)(Schizophrenia Working Group of the Psychiatric Genomics Consortium, 2014), highest level of educational attainment (EduAttain)(Lee et al., 2018), and sleep duration (SleepDuration)(Dashti et al., 2019). The non-brain related traits measure genetic liability for lean body mass (LBM)(Zillikens et al., 2017), bone mineral density (BMD)(Kemp et al., 2017), and coronary artery disease (CAD)(Howson et al., 2017).

We estimated LD scores for each foreground set and corresponding background set with the LDSC regression pipeline `make_annot` and `ldsc` functions using `hg38` 1000 Genomes European Phase 3 European super-population (1000G EUR) cohort plink files downloaded from https://data.broadinstitute.org/alkesgroup/LDSCORE/GRCh38/. An example of an ATAC-seq optimal set of reproducible peaks mapped to `hg38` in narrowPeak format is annotated with 1000G EUR LD scores using the following call:

```
python make_annot.py \
--bed-file optimal_peak.narrowPeak.gz \
--bimfile 1000G.EUR.hg38.${chr}.bim \
--annot-file foreground.${chr}.annot
```

We downloaded the baseline v1.2 files for cell type-specific enrichment in `hg38` coordinates from the same link above as well as the corresponding weights

`weights.hm3_noMHC' file excluding the MHC region from https://data.broadinstitute.org/alkesgroup/LDSCORE/. HapMap SNPs and corresponding weights file used in the LDSC analyses only refer to the SNP rsIDs, rather than genomic coordinates, so only the baseline and LD statistics used to annotate the foreground and background files must be in `hg38` coordinates. In accordance with the LDSC regression script input format, we created an `enrichment.ldcts' file listing the annotated foreground/background pair for each foreground set. We estimated the partitioned heritability using the `ldsc` function, which integrates the foreground and background LD score estimates, munged GWAS SNP data, baseline variant data, and variants weights. The final function call to GWAS enrichment is as follows:

```
python ldsc.py --h2-cts $Munged_GWAS \
      --ref-ld-chr baseline_v1.2/baseline. \
      --w-ld-chr weights.hm3_noMHC. \
      --ref-ld-chr-cts enrichment.ldcts \
      --out $Output_Label
```

The pipeline produced LD score regression coefficient, coefficient error, and coefficient p-value estimates. We adjusted for multiple testing using the false discovery rate on p-values of the LD score regression coefficients (`alpha = 0.05`) on all 18 GWAS traits intersected on within the same foreground/background set. A significant FDR-value indicates enrichment of the foreground genomic regions for GWAS SNPs relative to the background. Lastly, we computed genetic correlations in **Supplemental Figure 1A** between GWAS of addiction-associated traits using the pre-munged summary statistics as described by Bulik-Sullivan *et al.*(Bulik-Sullivan et al., 2015a)

Bulk tissue ATAC-seq

To augment and compare to mouse cell type-specific ATAC-seq datasets generated in this study, we also performed bulk tissue ATAC-seq from cortex (CTX) and dorsal striatum/nucleus accumbens (CPU) of 7- and 12-week-old C57Bl/6J mice (N = 2 each age) as described in Buenrostro *et al.*, 2015(Buenrostro et al., 2015) with the following minor differences in buffers and reagents. We euthanized mice with isoflurane, rapidly decapitated to extract the brain, and sectioned it in ice-cold oxygenated aCSF (119mM NaCl, 2.5 mM KCl, 1mM NaH_2PO_4(monobasic), 26.2mM $NaHCO_3$, 11mM glucose) at 200-micron sections on a vibratome (Leica VT1200). We further micro-dissected sections for cortex and dorsal striatum on a stereo microscope and transferred dissected regions into chilled lysis buffer (Buenrostro et al., 2015). We dounce homogenized the dissected brains in 5mL of lysis buffer with the loose pestle (pestle A) in a 15mL glass dounce homogenizer (Pyrex #7722-15). We washed nuclei lysate off the pestle with 5mL of lysis buffer and filtered the nuclei through a 70-micron cell strainer into a 50mL conical tube. We washed the dounce homogenizer again with 10mL of BL buffer and transferred the lysate through the 70-micron filter (Foxx 1170C02). We pelleted the 20 mL of nuclei lysate at 2,000 x *g* for 10 minutes in a refrigerated centrifuge at 4°C. We discarded the supernatant and resuspended the nuclei in 100-300 microliters of water to approximate a concentration of 1-2 million nuclei/ mL. We filtered the nuclei suspension through a 40-micron cell strainer. We stained a sample of nuclei with DAPI (Invitrogen #D1206) and counted the sample to measure 50k nuclei per ATAC-seq transposition reaction. The remaining steps follow the Buenrostro *et al.*, 2015(Buenrostro et al., 2015) protocol for tagmentation and library amplification. We shallowly sequenced barcoded ATAC-seq libraries at 1-5 million reads per sample on an Illumina MiSeq and processed individual samples through the ENCODE pipeline for initial quality control. We used these QC measures

(clear periodicity, library complexity, and minimal bottlenecking) to filter out low-quality samples and re-pooled a balanced library for paired-end deep sequencing on an Illumina NextSeq to target 30 million uniquely mapped fragments per sample after mitochondrial DNA and PCR duplicate removal. These raw sequencing files entered processing through the ENCODE ATAC-seq pipeline as above by merging technical replicates and grouping biological replicates by brain region for each pipeline run.

Cre-Specific Nuclear-Anchored Independent Labeling (cSNAIL) virus procedures

The cSNAIL genome (pAAV-Ef1a-DIO-Sun1-Gfp-WPRE-pA) contains *loxP* sites to invert the *Sun1-Gfp* fusion gene and integrate into the nuclear membrane of cells expressing the *Cre* gene, allowing these cell populations to be profiled for various genomic assays (Lawler et al, 2020 in press J. Neuro). We packaged the cSNAIL genome with AAV variant PHP.eB (pUCmini-iCAP-PHP.eB) in AAVpro(R) 293T cells (Takara, cat #632273). Viviana Gradinaru provided us with the pUCmini-iCAP-PHP.eB (http://n2t.net/addgene:103005; RRID: Addgene 103005)(Chan et al., 2017). We precipitated viral particles with polyethylene glycol, isolated with ultracentrifugation on an iodixanol density gradient, and purified in PBS with centrifugation washes and 0.2µM syringe filtration. We injected each mouse with 4.0 x 10^{11}vg into the retro-orbital cavity under isoflurane anesthesia. We allowed the virus to incubate in the animal for 3-4 weeks to reach peak expression. We closely monitored the health of the animals throughout the length of the virus incubation and did not note any concerns.

cSNAIL nuclei isolation

On the day of the ATAC-seq experiments, we dissected brain regions from fresh tissue and extracted nuclei in the same manner as described for bulk tissue experiments. Then, we sorted the nuclei suspension into Sun1GFP+ (Cre+) and Sun1GFP- (Cre-) fractions using affinity purification

with Protein G Dynabeads (Thermo Fisher, cat. 10004D). A pre-clearing incubation with beads and nuclei for 10-15 minutes removes effects from non-specific binding events. Next, we incubated the remaining free nuclei with anti-GFP antibody (Invitrogen, #G10362) for 30 minutes to bind Sun1GFP. Finally, we added new beads to the solution to conjugate with the antibody and incubated the reaction for an additional 20 minutes. The pre-clear step and all incubations took place in wash buffer (0.25M Sucrose, 25mM KCl, 5mM $MgCl_2$, 20mM Tricine with KOH to pH 7.8, and 0.4% IGEPAL) at 4°C with end-to-end rotation. After the binding process, we separated bead-bound nuclei on a magnet, washed three times with wash buffer, and filtered through a 20µM filter to ensure purity. We resuspended nuclei in nuclease-free water for input into the ATAC-seq tagmentation reaction. We performed nuclei quantification and tagmentation in the same manner described for bulk tissue ATAC-seq above. We list in the table below the number of animals, the genotypes, and which regions collected for ATAC-seq experiments in this study. N=2 *Pvalb-cre* samples from CPU/NAc region had received a sham surgery with saline injection into the external globus pallidus 5 days before they were sacrificed (Lawler et al, 2020 in press J. Neuro.) N=2 *Drd1-cre* samples from both CPU and NAc regions had received headcap surgeries 3 weeks before they were sacrificed. Both *Pvalb-cre* and *Drd1-cre* were overall healthy at time of sacrifice.

Genotype	**Replicates**	**Sex** (**F**emale /**M**ale)	**Region and Replicate per region**	**Cell type**
C57BL/6 WT	N=4	2 F, 2 M	CTX= 4, CPU/NAc = 4	bulk
Pvalb-cre	N=5	3 F (CTX) 1 F, 1 M (CPU/NAc)	CTX= 3, CPU/NAc = 2	PV
Sst-cre	N=2	1 F, 1 M	CTX= 2, CPU/NAc = 2	SST
Drd1-cre	N=2	2 F	CPU=2, NAc=2	D1
Adora2a-cre	N=2	2 F	CPU=2, NAc=2	D2

cSNAIL Cell Type Specificity

We created a consensus set of non-overlapping IDR peaks from the ATAC-seq pipeline for cSNAIL ATAC-seq and Mo *et al.* INTACT samples (`Tissue`: Ctx, Cpu, and NAc ; `Celltype`: EXC, PV, SST, VIP, D1, D2). We extended the peak set 200bp up- and down-stream, count overlapping fragments with `Rsubread v2.0.1` using the de-duplicated BAM files from the pipeline(Liao et al., 2014), and created with `DESeq2 v1.26.0` a variance-stabilized count matrix aware of experimental `Group` (combination of `Tissue` and `Celltype`) with `~Group` (Love et al., 2014). We plotted the principle component analysis in **Supplemental Figure 3A** for the first two components with this variance-stabilized count matrix. We used `Deeptools v3.5.0` to convert the same BAM files to normalized bigWig files and average over replicates of the same `Group`(Ramírez et al., 2016), We plotted the tracks using `pyGenomeTracks v3.5` around marker genes for each cell type (*Slc17a7*, *Drd1*, *Adora2a*, *Pvalb*, *Sst*, *Vip*)(Ramírez et al., 2018) **Supplemental Figure 3B**. We computed the mean accessibility for each `Group` 2kb up- and down-stream the transcription start sites (TSS) and correlated $\log_{10}$(TSS accessibility + 1) with gene expression $\log_{10}$(meta gene counts + 1) of Drop-Seq annotated cell types from prefrontal cortex and striatum(Saunders et al., 2018). We used the Saunders *et al.* tissue subcluster metagene profiles (sum of gene expression in all cells) and summed subclusters to cluster-level metagene profiles. Most tissue cluster metagene profiles corresponded to cSNAIL ATAC-seq celltype and tissue profiles, with the exception of cSNAIL cortical PV+ samples were matched to Saunders *et al.* cortical MGE+ interneuron clusters.

Convolutional Neural Network models for CRE cell type classification

We trained a set of convolutional neural network (CNN) models to learn the regulatory grammar of a given cell type from the DNA sequences underlying the cell type's OCRs. The models take in

one-hot encoded 501bp genomic sequences, where positives are centered on the IDR peak summits that are annotated to be in introns and distal intergenic regions and negatives are approximately ten times the number of positives sequences that are G/C-matched and not overlapping IDR peaks, to predict 1 for an OCR or 0 for negative sequence. We excluded promoters (defined as within 5,000bp from the TSS) and exons since distal sequences have been shown to confer more cell type-specificity and be more predictive of expression levels of regulated genes (Roadmap Epigenomics Consortium et al., 2015). We constructed the negative set by first building a sequence repository `$BGDIR` according to https://bitbucket.org/CBGR/biasaway_background_construction/src/master/ from the mouse `mm10` genome using 501bp sequences. Then we used the `biasaway`(Worsley Hunt et al., 2014; Khan et al., 2020) command-line interface-generated negative sequences with the matching nucleotide distribution along a sliding window along the 501bp IDR peak sequence:

```
biasaway c --foreground $FGFASTA --nfold 10 --deviation 2.6 --step 50 --seed 1 -winlen 100 --bgdirectory $BGDIR
```

We employed a 5-fold cross validation chromosome hold-out scheme to train 5 models per set of IDR peaks to ensure stable and consistently learned regulatory patterns. A model for training a fold does not see sequences during training from the validation set for that fold, and no models see the test set until final model performance evaluation. Sequences from these chromosomes were used as the validation set for each fold:

fold1: {chr6, chr13, chr21}

fold2: {chr7, chr14, chr18}

fold3: {chr11, chr17, chrX}

fold4: {chr9, chr12}

fold5: {chr10, chr8}.

We used sequences from chromosomes {chr1, ch2, chr19} for the test set.

We trained the models with Keras v2.3.0-tf (https://keras.io/) implemented through Tensorflow v2.2.0 and used stochastic gradient descent (SGD) with Nesterov momentum to minimize the binary cross entropy loss and learn model parameters. All models used the same CNN architecture with five consecutive Conv2D layers (conv_width = 11, conv_height = 4, conv_filters = 200, stride = 1), one MaxPooling2D layer (max_pool_size = 26, max_pool_stride = 26), one Dense layer (dense_filters = 300), one Dropout layer (proportion_dropout = .1), and a final output Dense layer (activation = 'sigmoid'). All Conv2D and Dense used the 'relu' activation and L2 regularization (l2_reg = 1e-10), unless otherwise stated. We applied the One-Cycle-Policy (OCP) with linear cyclical learning rate and momentum between a base and max rates as described previously (Smith, 2018) to train each fold with batch size= 2000, epochs = 23, num_cycles = 2.35, base_learning_rate = 1e-2, max_learning_rate = 1e-1, base_momentum = .85, max_momentum = 0.99. These parameters robustly and efficiently trained models across folds to accurately predict positive OCRs of all cell types against an approximately 1:10 positive:negative class imbalance. We computed classifier performance metrics including weighted accuracy (using threshold = 0.5), weighted f1_score (using threshold = 0.5), area under receiver operating characteristic (auROC), and area under precision-recall curve (auPRC). We provide the scripts and .h5 files with Keras model architectures and weights on the GitHub page https://github.com/pfenninglab/addiction_gwas_enrichment.

779

780 **Machine learning cell type-specific prioritization of *Fullard et al.* NeuN+ ATAC-seq peaks**

781 We used CNN model scores to classify whether a peak from *Fullard et al*. NeuN+ open chromatin
782 data is active in a neuronal subtype {`EXC, D1, D2`}. We took NeuN+ IDR "optimal peaks"
783 from regions significantly enriched for addiction-associated traits {`OFC, VLPFC, DLPFC,`
784 `ACC, STC, PUT, NAc`, **Figure 1A**}, extracted 501bp DNA sequences of each centered on the
785 summit, and scored each peak with cell type-specific machine learning models trained with the
786 appropriate tissue context (e.g. score cortical NeuN+ peaks with a model trained with cortical EXC
787 cell type). We averaged scores across model folds from the same cell types and classified NeuN+
788 peaks with scores greater than `0.5` as active in that cell type. We defined these ML-prioritized
789 peaks as foregrounds for LDSC regression GWAS enrichment analyses as described above. We
790 created a consensus set of peaks merging all model-prioritized peaks and the Honeybadger2 set of
791 OCRs to be the matched background, and we performed GWAS enrichment and computed FDR
792 on all 18 GWAS traits (only enrichments for addiction-associated GWAS shown, **Figure 3**).

793

794 **Addiction-associated GWAS processing and cell type-specific candidate selection**

795 We collected the addiction-associated SNPs by submitting the summary statistics files for the
796 seven addiction-associated traits{`AgeofInitiation` (Liu et al., 2019b),
797 `CigarettesPerDay` (Liu et al., 2019b), `SmokingInitiation` (Liu et al., 2019b),
798 `SmokingCessation` (Liu et al., 2019b), `DrinksPerWeek` (Liu et al., 2019b), `Cannabis`
799 (Pasman et al., 2018), `RiskyBehavior` (Karlsson Linnér et al., 2019)} to the FUMA webserver
800 (Watanabe et al., 2017). FUMA computed LD R^2 based on the 1000 Genomes European (1000G
801 EUR) super-population reference (1000 Genomes Project Consortium et al., 2015) via PLINK

(Purcell et al., 2007), linked GWAS-significant lead SNPs to off-lead SNPs in LD with the lead, and annotated functional consequences of genetic variants via ANNOVAR based on ENSEMBL build 85 human gene annotations (Wang et al., 2010) **(Figure 1A)**. ANNOVAR functional gene annotations for a SNP are as defined in the primary publication and online: `https://annovar.openbioinformatics.org/en/latest/user-guide/gene/`. The aggregate of 14,790 unique SNPs span 215 genomic loci. We limited ourselves SNPs that overlapped Fullard *et al.* NeuN+ OCRs (Fullard et al., 2018) since nucleotide variants in these peaks may disrupt epigenomic DNA sequences measured by ATAC-seq. We also limited ourselves SNPs that are fine-mapped and predicted to be causal by CAUSALdb using the European LD structure and an ensemble of statistical fine-mapping tools (FINEMAP, CAVIARBF, PAINTOR) (Chen et al., 2015; Benner et al., 2016; Kichaev et al., 2017; Wang et al., 2020). Combining these two filtering heuristics, being in NeuN+ OCRs and fine-mapped putatively causal, narrowed us down to 170 SNPs over 54 loci to be further refined for cell type-specific activity.

We further filtered the 170 SNPs to only those overlapping OCRs from cortical and striatal brain regions are enriched for addiction-associated variants { `OFC, DLPFC, VLPFC, ACC, STC, PUT, NAc`} (**Figure 1A**), and scored the filtered SNPs with ML models trained on mouse cortical or striatal cell type-specific ATAC-seq. We inputted DNA sequences of 501 bp centered at the SNP location for both the effect and non-effect allele into the ML models for predicting cell type-specific OCR activity and, for each cell type, computed the average cell type score (prediction) across models from different folds for each of the effect and non-effect alleles. To predict a measure of functional impact of the effect allele, we computed a SNP delta score ($score_{effect}$ $-score_{non\text{-}effect}$). Most SNPs reported by GWAS are not expected to be the

causal variant for a trait, so the distribution of cell type-specific model scores on the full list of 14,790 SNPs can be used to define a null distribution. From the 170 SNPs, we predict whether a SNP might have functional impact in cell type if either allele has a score > `0.5` and if the delta score magnitude is > `0.05`, the standard deviation of null delta scores. To accompany cell type-specific activity predictions, we downloaded SNPs that are reported *cis* expression quantitative trait loci (eQTL) in human cortex, frontal cortex (DLPFC), ACC, caudate, putamen, and NAc from the GTEX Consortium from `https://www.gtexportal.org/home/datasets(GTEx Consortium, 2013, 2015)`. We identified genes for which at least one of the 170 SNPs is an eQTL and plotted them as arcs in **Figure 4B** and **Supplemental Figure 4**. Locus plots are generated with `pyGenomeTracks v3.5` tools (Ramírez et al., 2018).

For **Figure 4A**, we compared SNP scores of the effect allele across each model and grouped them by whether they overlapped a cortical or striatal NeuN+ OCR, NeuN- OCR, both, or neither, depending on whether the model was for `EXC` or `D1/D2` cell types, respectively. We computed 2-tailed t-tests between groups and corrected for multiple comparisons with the family-wise Bonferroni method for N=18 tests from three models and (4 choose 2) six possible comparisons per model. * $P < 0.05/N$, ** $P < 0.01/N$, *** $P < 0.001/N$.

DATA AVAILABILITY

Code used to run intermediate and final analyses reported in this paper are available on the GitHub page: https://github.com/pfenninglab/addiction_gwas_enrichment. Sequencing output files for data generated in this study are deposited on the GEO at accession

XXXXX. Questions and comments about data and analyses may be directed to the corresponding author.

Bibliography

1000 Genomes Project Consortium, Auton A, Brooks LD, Durbin RM, Garrison EP, Kang HM, Korbel JO, Marchini JL, McCarthy S, McVean GA, Abecasis GR (2015) A global reference for human genetic variation. Nature 526:68–74.

Alipanahi B, Delong A, Weirauch MT, Frey BJ (2015) Predicting the sequence specificities of DNA- and RNA-binding proteins by deep learning. Nat Biotechnol 33:831–838.

Barman P, Reddy D, Bhaumik SR (2019) Mechanisms of Antisense Transcription Initiation with Implications in Gene Expression, Genomic Integrity and Disease Pathogenesis. Noncoding RNA 5.

Beaulieu C (1993) Numerical data on neocortical neurons in adult rat, with special reference to the GABA population. Brain Res 609:284–292.

Benner C, Spencer CCA, Havulinna AS, Salomaa V, Ripatti S, Pirinen M (2016) FINEMAP: efficient variable selection using summary data from genome-wide association studies. Bioinformatics 32:1493–1501.

Berke JD, Hyman SE (2000) Addiction, dopamine, and the molecular mechanisms of memory. Neuron 25:515–532.

Bracci E, Centonze D, Bernardi G, Calabresi P (2002) Dopamine excites fast-spiking interneurons in the striatum. J Neurophysiol 87:2190–2194.

Buenrostro JD, Giresi PG, Zaba LC, Chang HY, Greenleaf WJ (2013) Transposition of native chromatin for fast and sensitive epigenomic profiling of open chromatin, DNA-binding proteins and nucleosome position. Nat Methods 10:1213–1218.

Buenrostro JD, Wu B, Chang HY, Greenleaf WJ (2015) ATAC-seq: A Method for Assaying Chromatin Accessibility Genome-Wide. Curr Protoc Mol Biol 109:21.29.1-21.29.9.

Bulik-Sullivan B, Finucane HK, Anttila V, Gusev A, Day FR, Loh P-R, ReproGen Consortium, Psychiatric Genomics Consortium, Genetic Consortium for Anorexia Nervosa of the Wellcome Trust Case Control Consortium 3, Duncan L, Perry JRB, Patterson N, Robinson EB, Daly MJ, Price AL, Neale BM (2015a) An atlas of genetic correlations across human diseases and traits. Nat Genet 47:1236–1241.

Bulik-Sullivan B, Loh P-R, Finucane HK, Ripke S, Yang J, Schizophrenia Working Group of the Psychiatric Genomics Consortium, Patterson N, Daly MJ, Price AL, Neale BM (2015b) LD Score regression distinguishes confounding from polygenicity in genome-wide association studies. Nat Genet 47:291–295.

Bush WS, Moore JH (2012) Chapter 11: Genome-wide association studies. PLoS Comput Biol 8:e1002822.

Cabana-Domínguez J, Shivalikanjli A, Fernàndez-Castillo N, Cormand B (2019) Genome-wide association meta-analysis of cocaine dependence: Shared genetics with comorbid conditions. Prog Neuropsychopharmacol Biol Psychiatry 94:109667.

Cannon ME, Currin KW, Young KL, Perrin HJ, Vadlamudi S, Safi A, Song L, Wu Y, Wabitsch M, Laakso M, Crawford GE, Mohlke KL (2019) Open Chromatin Profiling in Adipose Tissue Marks Genomic Regions with Functional Roles in Cardiometabolic Traits. G3 (Bethesda) 9:2521–2533.

Chan KY, Jang MJ, Yoo BB, Greenbaum A, Ravi N, Wu W-L, Sánchez-Guardado L, Lois C, Mazmanian SK, Deverman BE, Gradinaru V (2017) Engineered AAVs for efficient noninvasive gene delivery to the central and peripheral nervous systems. Nat Neurosci 20:1172–1179.

Chen L, Fish AE, Capra JA (2018) Prediction of gene regulatory enhancers across species

894 reveals evolutionarily conserved sequence properties. PLoS Comput Biol 14:e1006484.
895 Chen W, Larrabee BR, Ovsyannikova IG, Kennedy RB, Haralambieva IH, Poland GA, Schaid
896 DJ (2015) Fine Mapping Causal Variants with an Approximate Bayesian Method Using
897 Marginal Test Statistics. Genetics 200:719–736.
898 Cheng Y, Huang CCY, Ma T, Wei X, Wang X, Lu J, Wang J (2017) Distinct synaptic
899 strengthening of the striatal direct and indirect pathways drives alcohol consumption.
900 Biol Psychiatry 81:918–929.
901 Cheng Z, Zhou H, Sherva R, Farrer LA, Kranzler HR, Gelernter J (2018) Genome-wide
902 Association Study Identifies a Regulatory Variant of RGMA Associated With Opioid
903 Dependence in European Americans. Biol Psychiatry 84:762–770.
904 Coffee and Caffeine Genetics Consortium et al. (2015) Genome-wide meta-analysis identifies six
905 novel loci associated with habitual coffee consumption. Mol Psychiatry 20:647–656.
906 Dashti HS et al. (2019) Genome-wide association study identifies genetic loci for self-reported
907 habitual sleep duration supported by accelerometer-derived estimates. Nat Commun
908 10:1100.
909 Davis CA, Hitz BC, Sloan CA, Chan ET, Davidson JM, Gabdank I, Hilton JA, Jain K,
910 Baymuradov UK, Narayanan AK, Onate KC, Graham K, Miyasato SR, Dreszer TR,
911 Strattan JS, Jolanki O, Tanaka FY, Cherry JM (2018) The Encyclopedia of DNA
912 elements (ENCODE): data portal update. Nucleic Acids Res 46:D794–D801.
913 Dick DM (2016) The genetics of addiction: where do we go from here? J Stud Alcohol Drugs
914 77:673–675.
915 Eddie D, Greene MC, White WL, Kelly JF (2019) Medical burden of disease among individuals
916 in recovery from alcohol and other drug problems in the united states: findings from the
917 national recovery survey. J Addict Med 13:385–395.
918 ENCODE Project Consortium (2012) An integrated encyclopedia of DNA elements in the
919 human genome. Nature 489:57–74.
920 Erzurumluoglu AM et al. (2019) Meta-analysis of up to 622,409 individuals identifies 40 novel
921 smoking behaviour associated genetic loci. Mol Psychiatry.
922 Farrell MR, Schoch H, Mahler SV (2018) Modeling cocaine relapse in rodents: Behavioral
923 considerations and circuit mechanisms. Prog Neuropsychopharmacol Biol Psychiatry
924 87:33–47.
925 Fehr C, Yakushev I, Hohmann N, Buchholz H-G, Landvogt C, Deckers H, Eberhardt A, Kläger
926 M, Smolka MN, Scheurich A, Dielentheis T, Schmidt LG, Rösch F, Bartenstein P,
927 Gründer G, Schreckenberger M (2008) Association of low striatal dopamine d2 receptor
928 availability with nicotine dependence similar to that seen with other drugs of abuse. Am J
929 Psychiatry 165:507–514.
930 Ferguson SM, Eskenazi D, Ishikawa M, Wanat MJ, Phillips PEM, Dong Y, Roth BL, Neumaier
931 JF (2011) Transient neuronal inhibition reveals opposing roles of indirect and direct
932 pathways in sensitization. Nat Neurosci 14:22–24.
933 Finucane HK et al. (2015) Partitioning heritability by functional annotation using genome-wide
934 association summary statistics. Nat Genet 47:1228–1235.
935 Finucane HK et al. (2018) Heritability enrichment of specifically expressed genes identifies
936 disease-relevant tissues and cell types. Nat Genet 50:621–629.
937 Fullard JF, Hauberg ME, Bendl J, Egervari G, Cirnaru M-D, Reach SM, Motl J, Ehrlich ME,
938 Hurd YL, Roussos P (2018) An atlas of chromatin accessibility in the adult human brain.
939 Genome Res 28:1243–1252.

940 GBD 2016 Alcohol and Drug Use Collaborators (2018) The global burden of disease attributable
941 to alcohol and drug use in 195 countries and territories, 1990-2016: a systematic analysis
942 for the Global Burden of Disease Study 2016. Lancet Psychiatry 5:987–1012.
943 Ghandi M, Lee D, Mohammad-Noori M, Beer MA (2014) Enhanced regulatory sequence
944 prediction using gapped k-mer features. PLoS Comput Biol 10:e1003711.
945 Gjoneska E, Pfenning AR, Mathys H, Quon G, Kundaje A, Tsai L-H, Kellis M (2015)
946 Conserved epigenomic signals in mice and humans reveal immune basis of Alzheimer's
947 disease. Nature 518:365–369.
948 Goldstein RZ, Volkow ND (2011) Dysfunction of the prefrontal cortex in addiction:
949 neuroimaging findings and clinical implications. Nat Rev Neurosci 12:652–669.
950 GTEx Consortium (2013) The Genotype-Tissue Expression (GTEx) project. Nat Genet 45:580–
951 585.
952 GTEx Consortium (2015) Human genomics. The Genotype-Tissue Expression (GTEx) pilot
953 analysis: multitissue gene regulation in humans. Science 348:648–660.
954 GTEx Consortium et al. (2017) Genetic effects on gene expression across human tissues. Nature
955 550:204–213.
956 Hickey G, Paten B, Earl D, Zerbino D, Haussler D (2013) HAL: a hierarchical format for storing
957 and analyzing multiple genome alignments. Bioinformatics 29:1341–1342.
958 Howson JMM et al. (2017) Fifteen new risk loci for coronary artery disease highlight arterial-
959 wall-specific mechanisms. Nat Genet 49:1113–1119.
960 International Obsessive Compulsive Disorder Foundation Genetics Collaborative (IOCDF-GC)
961 and OCD Collaborative Genetics Association Studies (OCGAS) (2018) Revealing the
962 complex genetic architecture of obsessive-compulsive disorder using meta-analysis. Mol
963 Psychiatry 23:1181–1188.
964 Jensen KP (2016) A Review of Genome-Wide Association Studies of Stimulant and Opioid Use
965 Disorders. Mol Neuropsychiatry 2:37–45.
966 Ji X, Saha S, Kolpakova J, Guildford M, Tapper AR, Martin GE (2017) Dopamine Receptors
967 Differentially Control Binge Alcohol Drinking-Mediated Synaptic Plasticity of the Core
968 Nucleus Accumbens Direct and Indirect Pathways. J Neurosci 37:5463–5474.
969 Jiang C, Wang X, Le Q, Liu P, Liu C, Wang Z, He G, Zheng P, Wang F, Ma L (2019) Morphine
970 coordinates SST and PV interneurons in the prelimbic cortex to disinhibit pyramidal
971 neurons and enhance reward. Mol Psychiatry.
972 Johnston KJA, Adams MJ, Nicholl BI, Ward J, Strawbridge RJ, Ferguson A, McIntosh AM,
973 Bailey MES, Smith DJ (2019) Genome-wide association study of multisite chronic pain
974 in UK Biobank. PLoS Genet 15:e1008164.
975 Kalita CA, Brown CD, Freiman A, Isherwood J, Wen X, Pique-Regi R, Luca F (2018) High-
976 throughput characterization of genetic effects on DNA-protein binding and gene
977 transcription. Genome Res 28:1701–1708.
978 Karlsson Linnér R et al. (2019) Genome-wide association analyses of risk tolerance and risky
979 behaviors in over 1 million individuals identify hundreds of loci and shared genetic
980 influences. Nat Genet 51:245–257.
981 Kelley DR, Reshef YA, Bileschi M, Belanger D, McLean CY, Snoek J (2018) Sequential
982 regulatory activity prediction across chromosomes with convolutional neural networks.
983 Genome Res 28:739–750.
984 Kelley DR, Snoek J, Rinn JL (2016) Basset: learning the regulatory code of the accessible
985 genome with deep convolutional neural networks. Genome Res 26:990–999.

Kemp JP et al. (2017) Identification of 153 new loci associated with heel bone mineral density and functional involvement of GPC6 in osteoporosis. Nat Genet 49:1468–1475.

Kendler KS, Prescott CA (1998a) Cannabis use, abuse, and dependence in a population-based sample of female twins. Am J Psychiatry 155:1016–1022.

Kendler KS, Prescott CA (1998b) Cocaine use, abuse and dependence in a population-based sample of female twins. Br J Psychiatry 173:345–350.

Khan A, Riudavets Puig R, Boddie P, Mathelier A (2020) BiasAway: command-line and web server to generate nucleotide composition-matched DNA background sequences. Available at: https://biasaway.uio.no [Accessed July 1, 2020].

Kichaev G, Roytman M, Johnson R, Eskin E, Lindström S, Kraft P, Pasaniuc B (2017) Improved methods for multi-trait fine mapping of pleiotropic risk loci. Bioinformatics 33:248–255.

Kim C, Kim S, Lee KY, Kim NH, Kang E-Y, Oh Y-W, Shin C (2019) Differences in bone density on chest CT according to smoking status in males without chronic obstructive lung disease. Sci Rep 9:10467.

Koob GF, Volkow ND (2010) Neurocircuitry of addiction. Neuropsychopharmacology 35:217–238.

Koob GF, Volkow ND (2016) Neurobiology of addiction: a neurocircuitry analysis. Lancet Psychiatry 3:760–773.

Krienen FM et al. (2019) Innovations in primate interneuron repertoire. BioRxiv.

Lake BB, Chen S, Sos BC, Fan J, Kaeser GE, Yung YC, Duong TE, Gao D, Chun J, Kharchenko PV, Zhang K (2018) Integrative single-cell analysis of transcriptional and epigenetic states in the human adult brain. Nat Biotechnol 36:70–80.

Landt SG et al. (2012) ChIP-seq guidelines and practices of the ENCODE and modENCODE consortia. Genome Res 22:1813–1831.

Lansink CS, Goltstein PM, Lankelma JV, Pennartz CMA (2010) Fast-spiking interneurons of the rat ventral striatum: temporal coordination of activity with principal cells and responsiveness to reward. Eur J Neurosci 32:494–508.

Lee D (2016) LS-GKM: a new gkm-SVM for large-scale datasets. Bioinformatics 32:2196–2198.

Lee IS, Leem AY, Lee SH, Rhee Y, Ha Y, Kim YS (2016) Relationship between pulmonary function and bone mineral density in the Korean National Health and Nutrition Examination Survey. Korean J Intern Med 31:899–909.

Lee JH, Ribeiro EA, Kim J, Ko B, Kronman H, Jeong YH, Kim JK, Janak PH, Nestler EJ, Koo JW, Kim J-H (2020) Dopaminergic regulation of nucleus accumbens cholinergic interneurons demarcates susceptibility to cocaine addiction. Biol Psychiatry.

Lee JJ et al. (2018) Gene discovery and polygenic prediction from a genome-wide association study of educational attainment in 1.1 million individuals. Nat Genet 50:1112–1121.

Lefort S, Tomm C, Floyd Sarria JC, Petersen CCH (2009) The excitatory neuronal network of the C2 barrel column in mouse primary somatosensory cortex. Neuron 61:301–316.

Liao Y, Smyth GK, Shi W (2014) featureCounts: an efficient general purpose program for assigning sequence reads to genomic features. Bioinformatics 30:923–930.

Liu C, Wang M, Wei X, Wu L, Xu J, Dai X, Xia J, Cheng M, Yuan Y, Zhang P, Li J, Feng T, Chen A, Zhang W, Chen F, Shang Z, Zhang X, Peters BA, Liu L (2019a) An ATAC-seq atlas of chromatin accessibility in mouse tissues. Sci Data 6:65.

Liu M et al. (2019b) Association studies of up to 1.2 million individuals yield new insights into the genetic etiology of tobacco and alcohol use. Nat Genet 51:237–244.

1032 Love MI, Huber W, Anders S (2014) Moderated estimation of fold change and dispersion for
1033 RNA-seq data with DESeq2. Genome Biol 15:550–550.
1034 Melé M et al. (2015) The human transcriptome across tissues and individuals. Science 348:660–
1035 665.
1036 Minnoye L, Taskiran II, Mauduit D, Fazio M, Van Aerschot L, Hulselmans G, Christiaens V,
1037 Makhzami S, Seltenhammer M, Karras P, Primot A, Cadieu E, van Rooijen E, Marine J-
1038 C, Egidy G, Ghanem GE, Zon L, Wouters J, Aerts S (2020) Cross-species analysis of
1039 enhancer logic using deep learning. Genome Res.
1040 Mo A, Mukamel EA, Davis FP, Luo C, Henry GL, Picard S, Urich MA, Nery JR, Sejnowski TJ,
1041 Lister R, Eddy SR, Ecker JR, Nathans J (2015) Epigenomic signatures of neuronal
1042 diversity in the mammalian brain. Neuron 86:1369–1384.
1043 Pasman JA et al. (2018) GWAS of lifetime cannabis use reveals new risk loci, genetic overlap
1044 with psychiatric traits, and a causal influence of schizophrenia. Nat Neurosci 21:1161–
1045 1170.
1046 Paten B, Earl D, Nguyen N, Diekhans M, Zerbino D, Haussler D (2011) Cactus: Algorithms for
1047 genome multiple sequence alignment. Genome Res 21:1512–1528.
1048 Pear VA, Ponicki WR, Gaidus A, Keyes KM, Martins SS, Fink DS, Rivera-Aguirre A,
1049 Gruenewald PJ, Cerdá M (2019) Urban-rural variation in the socioeconomic determinants
1050 of opioid overdose. Drug Alcohol Depend 195:66–73.
1051 Pelechano V, Steinmetz LM (2013) Gene regulation by antisense transcription. Nat Rev Genet
1052 14:880–893.
1053 Pullen E, Oser C (2014) Barriers to substance abuse treatment in rural and urban communities:
1054 counselor perspectives. Subst Use Misuse 49:891–901.
1055 Purcell S, Neale B, Todd-Brown K, Thomas L, Ferreira MAR, Bender D, Maller J, Sklar P, de
1056 Bakker PIW, Daly MJ, Sham PC (2007) PLINK: a tool set for whole-genome association
1057 and population-based linkage analyses. Am J Hum Genet 81:559–575.
1058 Ramírez F, Bhardwaj V, Arrigoni L, Lam KC, Grüning BA, Villaveces J, Habermann B, Akhtar
1059 A, Manke T (2018) High-resolution TADs reveal DNA sequences underlying genome
1060 organization in flies. Nat Commun 9:189.
1061 Ramírez F, Ryan DP, Grüning B, Bhardwaj V, Kilpert F, Richter AS, Heyne S, Dündar F,
1062 Manke T (2016) deepTools2: a next generation web server for deep-sequencing data
1063 analysis. Nucleic Acids Res 44:W160-5.
1064 Ribeiro EA et al. (2018) Transcriptional and physiological adaptations in nucleus accumbens
1065 somatostatin interneurons that regulate behavioral responses to cocaine. Nat Commun
1066 9:3149.
1067 Roadmap Epigenomics Consortium et al. (2015) Integrative analysis of 111 reference human
1068 epigenomes. Nature 518:317–330.
1069 Saunders A, Macosko EZ, Wysoker A, Goldman M, Krienen FM, de Rivera H, Bien E, Baum M,
1070 Bortolin L, Wang S, Goeva A, Nemesh J, Kamitaki N, Brumbaugh S, Kulp D, McCarroll
1071 SA (2018) Molecular Diversity and Specializations among the Cells of the Adult Mouse
1072 Brain. Cell 174:1015–1030.e16.
1073 Scaplen KM, Kaun KR (2016) Reward from bugs to bipeds: a comparative approach to
1074 understanding how reward circuits function. J Neurogenet 30:133–148.
1075 Schall TA, Wright WJ, Dong Y (2020) Nucleus accumbens fast-spiking interneurons in
1076 motivational and addictive behaviors. Mol Psychiatry.
1077 Schizophrenia Working Group of the Psychiatric Genomics Consortium (2014) Biological

1078 insights from 108 schizophrenia-associated genetic loci. Nature 511:421–427.
1079 Shlyueva D, Stampfel G, Stark A (2014) Transcriptional enhancers: from properties to genome-
1080 wide predictions. Nat Rev Genet 15:272–286.
1081 Smith LN (2018) A disciplined approach to neural network hyper-parameters: Part 1 -- learning
1082 rate, batch size, momentum, and weight decay. arXiv.
1083 Tak YG, Farnham PJ (2015) Making sense of GWAS: using epigenomics and genome
1084 engineering to understand the functional relevance of SNPs in non-coding regions of the
1085 human genome. Epigenetics Chromatin 8:57.
1086 Tepper JM, Koós T (2017) Gabaergic interneurons of the striatum. In: Handbook of basal
1087 ganglia structure and function, second edition, pp 157–178 Handbook of behavioral
1088 neuroscience. Elsevier.
1089 Tewhey R, Kotliar D, Park DS, Liu B, Winnicki S, Reilly SK, Andersen KG, Mikkelsen TS,
1090 Lander ES, Schaffner SF, Sabeti PC (2016) Direct Identification of Hundreds of
1091 Expression-Modulating Variants using a Multiplexed Reporter Assay. Cell 165:1519–
1092 1529.
1093 Thurman RE et al. (2012) The accessible chromatin landscape of the human genome. Nature
1094 489:75–82.
1095 Vockley CM, Guo C, Majoros WH, Nodzenski M, Scholtens DM, Hayes MG, Lowe WL, Reddy
1096 TE (2015) Massively parallel quantification of the regulatory effects of noncoding
1097 genetic variation in a human cohort. Genome Res 25:1206–1214.
1098 Volkow ND, Chang L, Wang G-J, Fowler JS, Ding Y-S, Sedler M, Logan J, Franceschi D,
1099 Gatley J, Hitzemann R, Gifford A, Wong C, Pappas N (2003) Low level of brain
1100 dopamine d_2 receptors in methamphetamine abusers: association with metabolism in the
1101 orbitofrontal cortex. Focus (Madison) 1:150–157.
1102 Volkow ND, Morales M (2015) The brain on drugs: from reward to addiction. Cell 162:712–
1103 725.
1104 Volkow ND, Wang GJ, Fowler JS, Logan J, Gatley SJ, Hitzemann R, Chen AD, Dewey SL,
1105 Pappas N (1997) Decreased striatal dopaminergic responsiveness in detoxified cocaine-
1106 dependent subjects. Nature 386:830–833.
1107 Volkow ND, Wang GJ, Fowler JS, Logan J, Hitzemann R, Ding YS, Pappas N, Shea C, Piscani
1108 K (1996) Decreases in dopamine receptors but not in dopamine transporters in alcoholics.
1109 Alcohol Clin Exp Res 20:1594–1598.
1110 Volkow ND, Wang G-J, Tomasi D, Baler RD (2013) Unbalanced neuronal circuits in addiction.
1111 Curr Opin Neurobiol 23:639–648.
1112 Waaktaar T, Kan K-J, Torgersen S (2018) The genetic and environmental architecture of
1113 substance use development from early adolescence into young adulthood: a longitudinal
1114 twin study of comorbidity of alcohol, tobacco and illicit drug use. Addiction 113:740–
1115 748.
1116 Wang GJ, Volkow ND, Fowler JS, Logan J, Abumrad NN, Hitzemann RJ, Pappas NS, Pascani K
1117 (1997) Dopamine D2 receptor availability in opiate-dependent subjects before and after
1118 naloxone-precipitated withdrawal. Neuropsychopharmacology 16:174–182.
1119 Wang J, Huang D, Zhou Y, Yao H, Liu H, Zhai S, Wu C, Zheng Z, Zhao K, Wang Z, Yi X,
1120 Zhang S, Liu X, Liu Z, Chen K, Yu Y, Sham PC, Li MJ (2020) CAUSALdb: a database
1121 for disease/trait causal variants identified using summary statistics of genome-wide
1122 association studies. Nucleic Acids Res 48:D807–D816.
1123 Wang K, Li M, Hakonarson H (2010) ANNOVAR: functional annotation of genetic variants

1124 from high-throughput sequencing data. Nucleic Acids Res 38:e164.
1125 Watanabe K, Taskesen E, van Bochoven A, Posthuma D (2017) Functional mapping and
1126 annotation of genetic associations with FUMA. Nat Commun 8:1826.
1127 Wilar G, Shinoda Y, Sasaoka T, Fukunaga K (2019) Crucial Role of Dopamine D2 Receptor
1128 Signaling in Nicotine-Induced Conditioned Place Preference. Mol Neurobiol 56:7911–
1129 7928.
1130 Wiltschko AB, Pettibone JR, Berke JD (2010) Opposite effects of stimulant and antipsychotic
1131 drugs on striatal fast-spiking interneurons. Neuropsychopharmacology 35:1261–1270.
1132 Worsley Hunt R, Mathelier A, Del Peso L, Wasserman WW (2014) Improving analysis of
1133 transcription factor binding sites within ChIP-Seq data based on topological motif
1134 enrichment. BMC Genomics 15:472.
1135 Xu Z, Liang Q, Song X, Zhang Z, Lindtner S, Li Z, Wen Y, Liu G, Guo T, Qi D, Wang M,
1136 Wang C, Li H, You Y, Wang X, Chen B, Feng H, Rubenstein JL, Yang Z (2018) SP8 and
1137 SP9 coordinately promote D2-type medium spiny neuron production by activating Six3
1138 expression. Development 145.
1139 Yue F et al. (2014) A comparative encyclopedia of DNA elements in the mouse genome. Nature
1140 515:355–364.
1141 Zeng X, Liu D, Zhao X, Chao L, Li Y, Li H, Li W, Gui L, Wu W (2019) Association of bone
1142 mineral density with lung function in a Chinese general population: the Xinxiang rural
1143 cohort study. BMC Pulm Med 19:239.
1144 Zhang X, Kaplow IM, Wirthlin M, Park TY, Pfenning AR (2020) HALPER facilitates the
1145 identification of regulatory element orthologs across species. Bioinformatics.
1146 Zhou J, Troyanskaya OG (2015) Predicting effects of noncoding variants with deep learning-
1147 based sequence model. Nat Methods 12:931–934.
1148 Zillikens MC et al. (2017) Large meta-analysis of genome-wide association studies identifies
1149 five loci for lean body mass. Nat Commun 8:80.
1150

Figure 1. Substance use and risky behavior GWAS risk variants enrich within reward region- and cell type-specific epigenomic profiles.

Partitioned LDSC regression (GWAS enrichment) finds enrichment of substance use and risky behavior traits in region-specific and cell type-specific open chromatin profiles of human postmortem brain. **(A)** Pie chart of ANNOVAR-annotated(Wang et al., 2010) SNP function of addiction-associated trait lead and off-lead SNPs in LD R^2> 0.8. Dark colors indicate un-transcribed/non-coding annotations, light for transcribed/exonic annotations. SNP annotation labels are according to ANNOVAR using ENSEMBL build 85 gene annotations (Methods). **(B)** GWAS enrichment false-discovery rates in ATAC-seq of 14 postmortem human brain regions coupled with NeuN-labeled fluorescence activated nuclei sorting(Fullard et al., 2018). Brain regions are stratified by cortical and subcortical regions, with cortical regions ordered frontal to caudal. Sorted cell types within each brain region are denoted by shape (blue triangle for NeuN+/neuronal, red circle for NeuN-/glial). FDR-adjustment was performed across all enrichments on the Fullard *et al.* dataset for Figure 1A and Figure 3: **Cell type-specific machine learning models refine human NeuN+ enrichments for substance use genetic risk GWAS.** **(A)** Scheme to predict cell type-specific activity of NeuN+ ATAC-seq peaks enriched from brain regions assayed in Fullard *et al*. (Fullard et al., 2018) using ML models trained on mouse cell-type specific ATAC-seq peaks. ML-predicted OCRs are input into GWAS enrichment. (**B)** Partitioned LD score regression of addiction associated traits in Fullard *et al.* NeuN+ OCRs predicted to be cell type-specific by machine learning models of open chromatin. Cell types are colored by the source mouse cell type-specific OCRs from **Error! Reference source not found.A**. Original enrichments from Figure 1A are reproduced in black. Bolded points are significant for FDR < 0.05.

Figure 4: Machine learning (ML) models for predicting cell type-specific open chromatin predict activity of addiction GWAS SNPs

(A) Cell type-activity prediction scores from the effect allele of genome-wide significant lead SNPs and off-lead SNPs in LD $R^2 > 0.8$. Activity scores for SNPs are stratified by overlap with Fullard *et al*. (Fullard et al., 2018) cortical or striatal NeuN+ and NeuN- peaks. Significance symbols denote Bonferroni-adjusted p-values from 2-tailed t-tests for N=18 possible pairwise comparisons, N.S. not significant, * $P < 0.05/N$, ** $P < 0.01/N$, *** $P < 0.001/N$. **(B)** Locus plot candidate SNP with predicted function SNP impact in EXC, D1, and D2 cell types. Genome tracks from top to bottom: NeuN+ MACS2 ATAC-seq foldchange signal of regions enriched in Figure 1A, SNP tracks showing SNP filtering criteria down to candidate functional SNP (Methods), gene annotation tracks from GENCODE GRCh38, eQTL link tracks of FDR-significant GTEX cis-eQTL from cortical and striatal brains, and mouse-human orthologous putative CREs mapped from cSNAIL ATAC-seq. NeuN+ ATAC-seq tracks and eQTL links are colored by source brain region as cortical (teal) or striatal (blue). Cell types colors label cortical excitatory neurons (EXC; red), D1 medium spiny neurons (D1; blue), or D2 medium spiny neurons (D2; green).

Figure 5 Summary of LDSC GWAS enrichments in human and mouse-human orthologous bulk tissue and cell type open chromatin

(A) Schematic of human NeuN-labeled bulk tissue and occipital cortex cell types from **Figure 1** for which addiction-associated genetic variants were significantly enriched (FDR < 0.05) in OCRs. Brain regions are labelled by the cell type that enriched (NeuN+ : blue box/shading; NeuN- : red box/shading) spatially along with the trait(s) for which OCRs were found significantly enriched

with risk variants. Occipital cortex cell types from **Figure 1C** (same color scheme) are listed along with the trait(s) for which OCRs were found significantly enriched with risk variants. **(B)** Schematic of addiction-associated genetic variants that share enrichments from human brain regions and neuronal subtypes in both human and mouse-human orthologous open chromatin. Brain graphic adapted from Fullard *et al*.(Fullard et al., 2018)

Supplemental Figure 1. Shared and unique genetic architecture of genetic risk variants of addiction-associated traits.

(A) LDSC genetic correlation (r_g) matrix of seven addiction-associated traits. FDR-significant correlations at shown in bold, non-significant in gray (FDR < 0.05). **(B)** Upset plot of genomic loci shared or unique to each addiction-associated trait. Genomic loci are identified by shared GWAS-significant SNPs and genomic region overlap.

Supplemental Figure . **(C)** GWAS enrichment false-discovery rates in single cell THS-seq OCRs of major cell clusters in occipital cortex(Lake et al., 2018). Cell types in brain regions that are enriched at FDR < 0.05 are plotted with bigger shapes and with black outlines. Traits assessed are age of smoking initiation (AgeofInitiation), average number of cigarettes per day for ever smokers (CigarettesPerDay), having ever regularly smoked (Smoking Initiation), current versus former smokers (SmokingCessation), number of alcoholic drinks per week (DrinksPerWeek)(Liu et al., 2019b), lifetime cannabis use (Cannabis)(Pasman et al., 2018), and risky behavior (RiskyBehavior)(Karlsson Linnér et al., 2019). OFC: orbitofrontal cortex, VLPFC: ventrolateral prefrontal cortex, DLPFC: dorsolateral prefrontal cortex, ACC: anterior cingulate cortex, INS:

insula, STC: superior temporal gyrus, ITC: inferior temporal gyrus, PMC: primary motor cortex, PVC: primary visual cortex, AMY: amygdala, HIPP: hippocampus, MDT: mediodorsal thalamus, NAc: nucleus accumbens, PUT: putamen, Ast: astrocyte, End: endothelial, Ex: excitatory neuron, In: inhibitory neuron, Mic: microglia, Oli: oligodendrocyte, Opc: oligodendrocyte precursor.

Figure 2: Cell type-specific enrichment of substance use traits are conserved in mouse-human orthologous open chromatin regions.

(A) Experimental design to map human orthologous regions from mouse ATAC-seq of bulk cortex (CTX), dorsal striatum (CPU), and nucleus accumbens (NAc) of cre-dependent Sun1-GFP Nuclear Anchored Independent Labeled (cSNAIL) nuclei of D1-cre, D2-cre, PV-cre, and SST-cre mice. cSNAIL ATAC-seq experiments report enriched (+) nuclei populations. **(B)** Partitioned LD score regression finds enrichment of substance use and risky behavior traits for brain region and cell type specific ATAC-seq open chromatin profiles of mouse brain. Replication of enrichment is shown using INTACT-enriched OCRs from Mo *et al*(Mo et al., 2015) of cortical excitatory (EXC+), vasoactive intestinal peptide interneuron (VIP+), and parvalbumin interneuron (PV+). Enrichments that are enriched at FDR < 0.05 are plotted with black outlines. FDR-adjusted p-value was performed across all mouse-human ortholog GWAS enrichment across Figure 2.

Figure 3: Cell type-specific machine learning models refine human NeuN+ enrichments for substance use genetic risk GWAS.

(A) Scheme to predict cell type-specific activity of NeuN+ ATAC-seq peaks enriched from brain regions assayed in Fullard *et al*. (Fullard et al., 2018) using ML models trained on mouse cell-type specific ATAC-seq peaks. ML-predicted OCRs are input into GWAS enrichment. (**B)** Partitioned

LD score regression of addiction associated traits in Fullard *et al.* NeuN+ OCRs predicted to be cell type-specific by machine learning models of open chromatin. Cell types are colored by the source mouse cell type-specific OCRs from **Error! Reference source not found.A**. Original enrichments from Figure 1A are reproduced in black. Bolded points are significant for FDR < 0.05.

Figure 4: Machine learning (ML) models for predicting cell type-specific open chromatin predict activity of addiction GWAS SNPs

(A) Cell type-activity prediction scores from the effect allele of genome-wide significant lead SNPs and off-lead SNPs in LD $R^2 > 0.8$. Activity scores for SNPs are stratified by overlap with Fullard *et al*. (Fullard et al., 2018) cortical or striatal NeuN+ and NeuN- peaks. Significance symbols denote Bonferroni-adjusted p-values from 2-tailed t-tests for N=18 possible pairwise comparisons, N.S. not significant, * $P < 0.05/N$, ** $P < 0.01/N$, *** $P < 0.001/N$. **(B)** Locus plot candidate SNP with predicted function SNP impact in EXC, D1, and D2 cell types. Genome tracks from top to bottom: NeuN+ MACS2 ATAC-seq foldchange signal of regions enriched in Figure 1A, SNP tracks showing SNP filtering criteria down to candidate functional SNP (Methods), gene annotation tracks from GENCODE GRCh38, eQTL link tracks of FDR-significant GTEX cis-eQTL from cortical and striatal brains, and mouse-human orthologous putative CREs mapped from cSNAIL ATAC-seq. NeuN+ ATAC-seq tracks and eQTL links are colored by source brain region as cortical (teal) or striatal (blue). Cell types colors label cortical excitatory neurons (EXC; red), D1 medium spiny neurons (D1; blue), or D2 medium spiny neurons (D2; green).

Figure 5 Summary of LDSC GWAS enrichments in human and mouse-human orthologous bulk tissue and cell type open chromatin

(A) Schematic of human NeuN-labeled bulk tissue and occipital cortex cell types from **Figure 1** for which addiction-associated genetic variants were significantly enriched (FDR < 0.05) in OCRs. Brain regions are labelled by the cell type that enriched (NeuN+ : blue box/shading; NeuN- : red box/shading) spatially along with the trait(s) for which OCRs were found significantly enriched with risk variants. Occipital cortex cell types from **Figure 1C** (same color scheme) are listed along with the trait(s) for which OCRs were found significantly enriched with risk variants. **(B)** Schematic of addiction-associated genetic variants that share enrichments from human brain regions and neuronal subtypes in both human and mouse-human orthologous open chromatin. Brain graphic adapted from Fullard *et al*.(Fullard et al., 2018)

Supplemental Figure 1. Shared and unique genetic architecture of genetic risk variants of addiction-associated traits.

(A) LDSC genetic correlation (r_g) matrix of seven addiction-associated traits. FDR-significant correlations at shown in bold, non-significant in gray (FDR < 0.05). **(B)** Upset plot of genomic loci shared or unique to each addiction-associated trait. Genomic loci are identified by shared GWAS-significant SNPs and genomic region overlap.

Supplemental Figure 2. Sensitivity of partitioned LDSC regression for cell type- and region-specific in the GWAS trait enrichment requires well-powered GWAS in relevant cell types.

GWAS enrichment plots with false-discovery rates in ATAC-seq of 14 postmortem human brain regions coupled with NeuN-labeled fluorescence activated nuclei sorting(Fullard et al., 2018). Regions are stratified by cortical and subcortical regions, with cortical regions ordered frontal to caudal. Sorted cell types within each brain region are denoted by shape (blue triangle for NeuN+/neuronal, red circle for NeuN-/glial). Cell types in brain regions that are enriched at FDR < 0.05 are plotted with bigger shapes and with black outlines. **(A)** GWAS enrichment of addiction- or substance use-associated traits: multi-site chronic pain (ChronicPain)(Johnston et al., 2019), cocaine dependence (CocaineDep)(Cabana-Domínguez et al., 2019) , opioid dependence (OpioidDep)(Cheng et al., 2018), diagnosis of obsessive-compulsive disorder (OCD)(International Obsessive Compulsive Disorder Foundation Genetics Collaborative (IOCDF-GC) and OCD Collaborative Genetics Association Studies (OCGAS), 2018), and cups of coffee drank per day (CoffeePerDay)(Coffee and Caffeine Genetics Consortium et al., 2015). The GWAS for OCD, opioid dependence, and cocaine dependence are reportedly underpowered to detect genetic liability for these traits (N_{case}< 5,000). **(B)** GWAS enrichment in well-powered brain-related traits show cell type- and region-specific enrichment: educational attainment (EduAttain)(Lee et al., 2018), schizophrenia risk (Schizophrenia)(Schizophrenia Working Group of the Psychiatric Genomics Consortium, 2014), habitual sleep duration (SleepDuration)(Dashti et al., 2019). **(C)** GWAS enrichment in non-brain associated traits do not show cell type- or region-specific enrichment: heel bone-mineral density (BMD)(Kemp et al., 2017), coronary artery disease (CAD)(Howson et al., 2017), and lean body mass (LBM)(Zillikens et al., 2017).

Supplemental Figure 3. Cell type specificity of cSNAIL ATAC-seq in mouse cortex and striatum

(A) Principle component plots of chromatin accessibility counts from cre-dependent Sun1-GFP Nuclear Anchored Independent Labeled (cSNAIL) ATAC-seq from *cre*-driver lines (**Methods**). Major axes of variation separate cell types by tissue source (PC1) and cell type versus bulk ATAC-seq (PC2). (B) Normalized coverage track plots around marker genes demarcating cell type-specificity of cSNAIL ATAC-seq samples. (C) Density correlation plot of normalized chromatin accessibility log counts around the transcription start site (TSS) with matched pseudo-bulk cell type log gene counts from Drop-seq of mouse cortex and striatum(Saunders et al., 2018). Drop-seq cell types meta-gene profiles report sum gene counts for cell clusters from frontal cortex and striatum. Pearson's and Spearman's correlation are denoted with R and ρ, respectively. (D) Pairwise correlation matrix of TSS chromatin accessibility log counts with Drop-seq pseudo-bulk log gene counts from cortical and striatal cell clusters.

Supplemental Figure 4. GWAS enrichment in addiction- and non-addiction-related traits using mapped mouse orthologs of tissue- and cell type-specific open chromatin regions.

GWAS enrichment plots with false-discovery rates in human orthologous regions mapped from mouse ATAC-seq of bulk cortex (CTX), dorsal striatum (CPU), and nucleus accumbens (Nac) or cre-dependent Sun1-GFP Nuclear Anchored Independent Labeled (cSNAIL) nuclei of D1-cre, D2-cre, and PV-cre mice. cSNAIL ATAC-seq experiments report both enriched (+) and de-enriched (-) nuclei populations. Enrichments that are enriched at FDR < 0.05 are plot with black outlines. Replication of enrichment is shown using INTACT-enriched OCRs from Mo *et al*(Mo et al., 2015) of cortical excitatory (EXC+), vasoactive intestinal peptide interneuron (VIP+), and parvalbumin interneuron (PV+). **(A)** GWAS enrichment of addiction- or substance use-associated traits: multi-site chronic pain (`ChronicPain`), cocaine dependence (`CocaineDep`), opioid dependence

(OpioidDep), diagnosis of obsessive-compulsive disorder (OCD), and cups of coffee drank per day (CoffeePerDay). The GWAS for OCD, opioid dependence, and cocaine dependence are reportedly underpowered to detect genetic liability for these traits (N_{case}< 5,000). **(B)** GWAS enrichment in well-powered brain-related traits show cell type- and region-specific enrichment: educational attainment (EduAttain), schizophrenia risk (Schizophrenia), habitual sleep duration (SleepDuration). **(C)** GWAS enrichment in non-brain associated traits do not show cell type- or region-specific enrichment: heel bone-mineral density (BMD), coronary artery disease (CAD), and lean body mass (LBM). **(D)** Heatmap of LDSC regression coefficients of GWAS enrichment for all measured GWAS in non-brain OCRs from human or mouse-human mapped orthologs. Tissues for which OCRs are significantly enriched (FDR < 0.05) with GWAS variants are outlined with a bolded box.

Supplemental Figure 5. ML model performance and selection of candidate functional SNPs. **(A)** Performance metrics for machine learning (ML) models evaluated on the test sets of IDR peaks or 10x nucleotide-distribution matched negatives. Five-fold cross validation scheme was used to train on IDR peaks of each cell type and tissue. Performance metrics are reported for accuracy and F1-score (using threshold = 0.5) and area under the receiver-operator-characteristic (auROC) and the precision-recall curve (auPRC) (**Methods**). Models were trained on IDR peaks of mouse cortical excitatory and striatal D1 and D2 medium spiny neurons. **(B)** Selection criteria from addiction-associated trait SNPs to candidate SNPs with functional impact in gene-regulatory function.

Supplemental Figure 6. Locus plots of addiction-associated SNPs predicted to act in striatal and cortical cell types.

(A-D) Locus plot of candidate SNP with predicted function SNP impact in D1 or D2 cell types. Genome tracks from top to bottom: NeuN+ MACS2 ATAC-seq foldchange signal of regions enriched in Figure 1A, SNP tracks showing SNP filtering criteria down to candidate functional SNP (Methods), gene annotation tracks from GENCODE GRCh38, eQTL link tracks of FDR-significant GTEX cis-eQTL from cortical and striatal brains, and mouse-human orthologous putative CREs mapped from cSNAIL ATAC-seq. NeuN+ ATAC-seq tracks and eQTL links are colored by source brain region as cortical (teal) or striatal (blue). Cell types colors label cortical excitatory neurons (EXC; red), D1 medium spiny neurons (D1; blue), D2 medium spiny neurons (D2; green). Panels A and C report SNPs that are known eQTLs in striatal brain tissues. (A) rs11191352 (SmokingInitiation), (B) rs10742814 (DrinksPerWeek), (C) rs9844736 (RiskyBehavior, SmokingInitiation), (D) Two SNPs ~400bp apart, rs6870603 and rs7712167 (SmokingInitiation).

Supplemental Table 1. Addiction-associated genetic variants annotated with cell type and brain region functional markers

Addiction-associated genetic variants from the seven GWAS explored in this study further annotated by FUMA(Watanabe et al., 2017), CAUSALdb(Wang et al., 2020), overlap with NeuN+ OCRs (Fullard et al., 2018), and ML model open chromatin prediction of the risk and non-risk alleles as well as ML model delta SNP scores. Several tabs report FUMA annotations, CAUSAL db annotation, SNP overlap with Fullard et al. NeuN+/NeuN- peaks, CNN scores for effect allele, CNN scores for non-effect allele, CNN delta SNP scores. All tabs contain unique identifying

columns according to FUMA outputs. Additional columns report HaploReg annotations from these SNPs where available data exists. The SNP positions are mapped to report hg38 coordinates and GenomicLocus report overlapping loci across. SNP overlaps with NeuN peaks are indicated as 0 for no overlap and 1 for overlap within IDR peaks. CNN scores are reported average across all folds and tissues from the same cell type and tissues. CNN scores range from 0 to 1, with scores larger than 0.5 are predicted active in that cell type. Delta SNP scores, instead, are normally distributed and centered at 0.

Functional Annotation of Addiction-associated GWAS SNPs

Figure 1

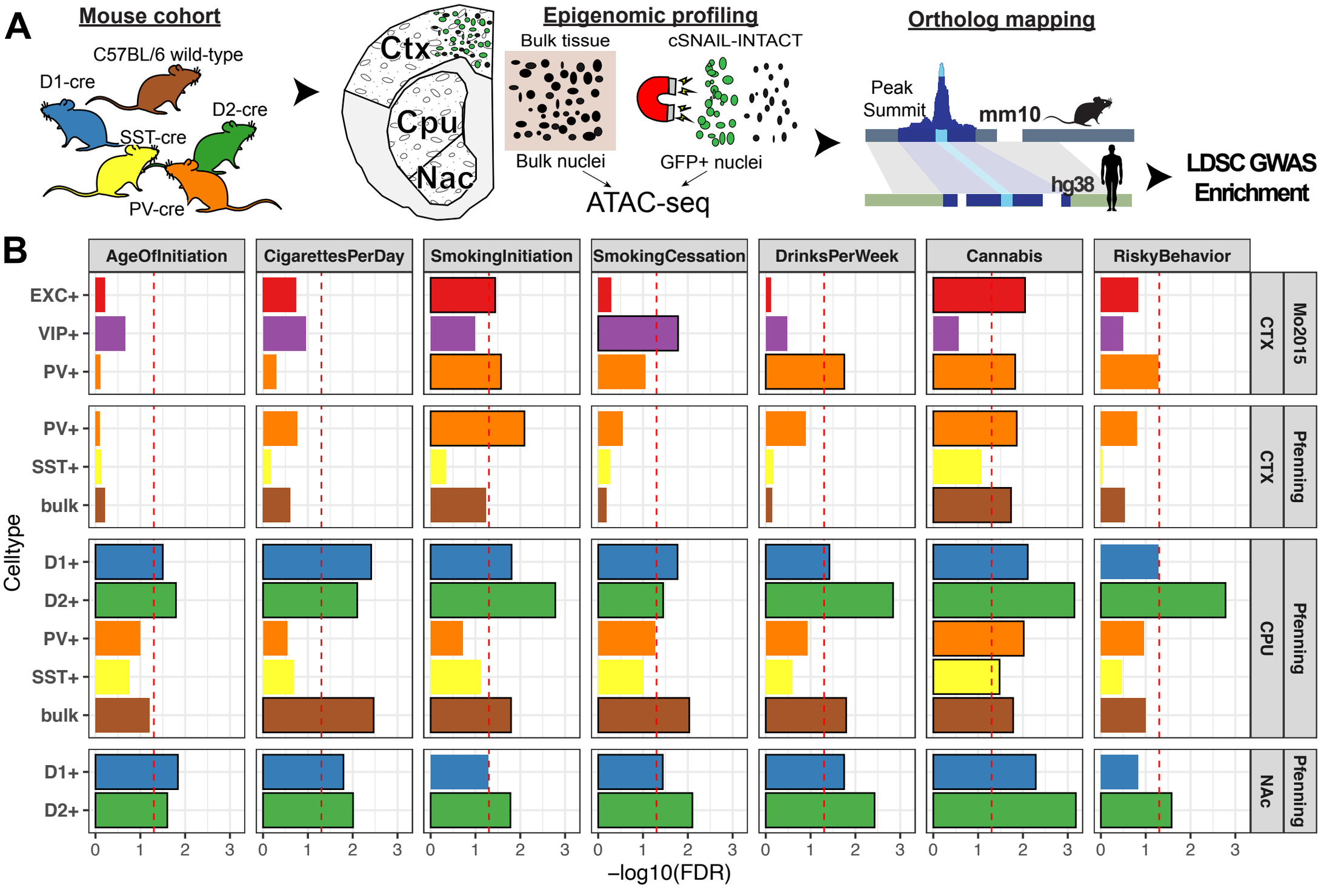
A
Mouse cohort
C57BL/6 wild-type
D1-cre
D2-cre
SST-cre
PV-cre
Ctx
Cpu
Nac
Epigenomic profiling
Bulk tissue
cSNAIL-INTACT
Bulk nuclei
GFP+ nuclei
ATAC-seq
Ortholog mapping
Peak
Summit
mm10
hg38
LDSC GWAS
Enrichment
B
AgeOfInitiation
CigarettesPerDay
SmokingInitiation
SmokingCessation
DrinksPerWeek
Cannabis
RiskyBehavior
CTX
Mo2015
Pfenning
CPU
NAc
EXC+
VIP+
PV+
SST+
bulk
D1+
D2+
Celltype
0
1
2
3
–log10(FDR)

Figure 2

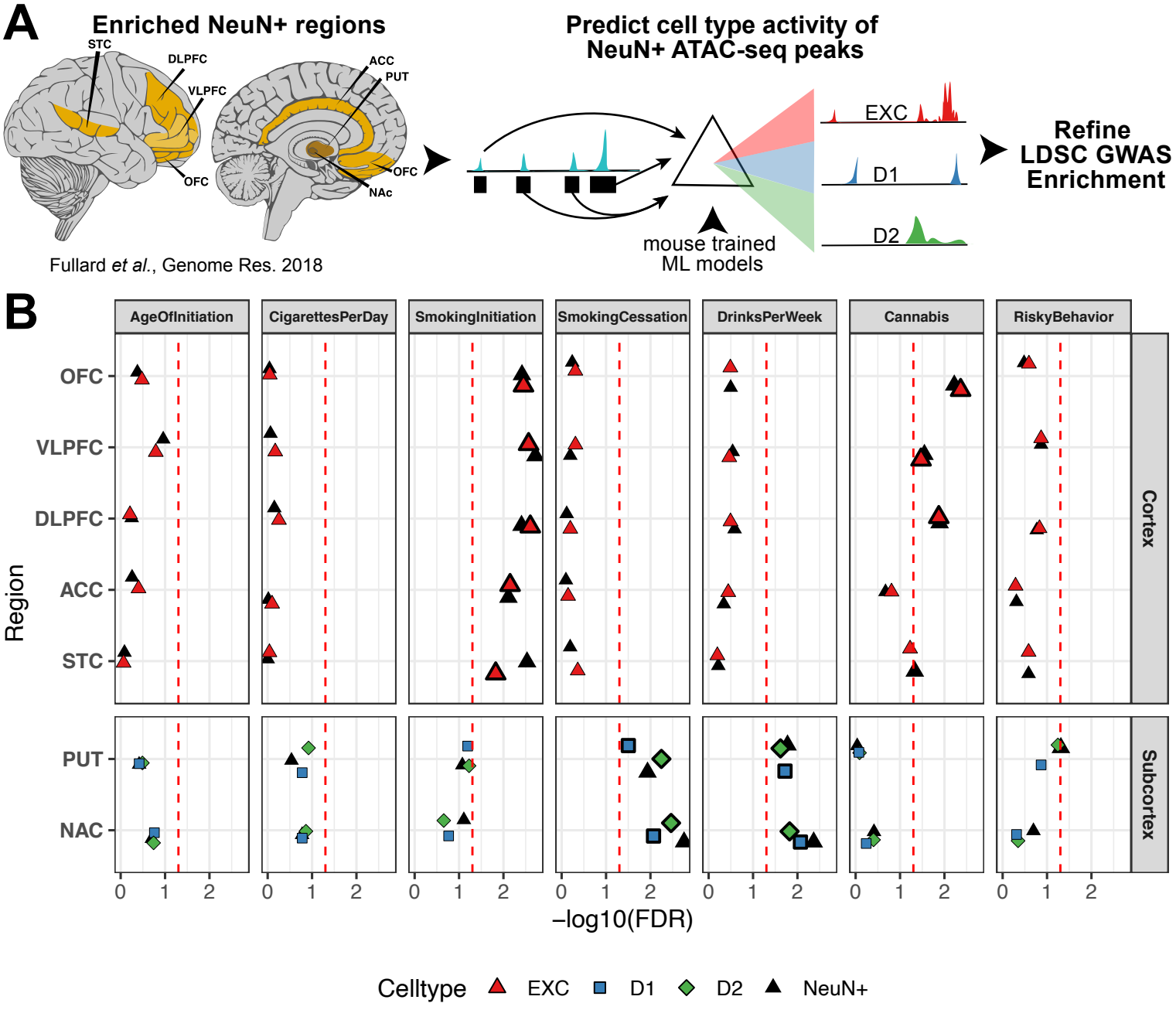
A
Enriched NeuN+ regions
STC
DLPFC
VLPFC
OFC
ACC
PUT
OFC
NAc
Fullard et al., Genome Res. 2018
Predict cell type activity of
NeuN+ ATAC-seq peaks
EXC
D1
D2
mouse trained
ML models
Refine
LDSC GWAS
Enrichment
B
AgeOfInitiation
CigarettesPerDay
SmokingInitiation
SmokingCessation
DrinksPerWeek
Cannabis
RiskyBehavior
Region
OFC
VLPFC
DLPFC
ACC
STC
PUT
NAC
Cortex
Subcortex
0
1
2
−log10(FDR)
Celltype
EXC
D1
D2
NeuN+

Figure 3

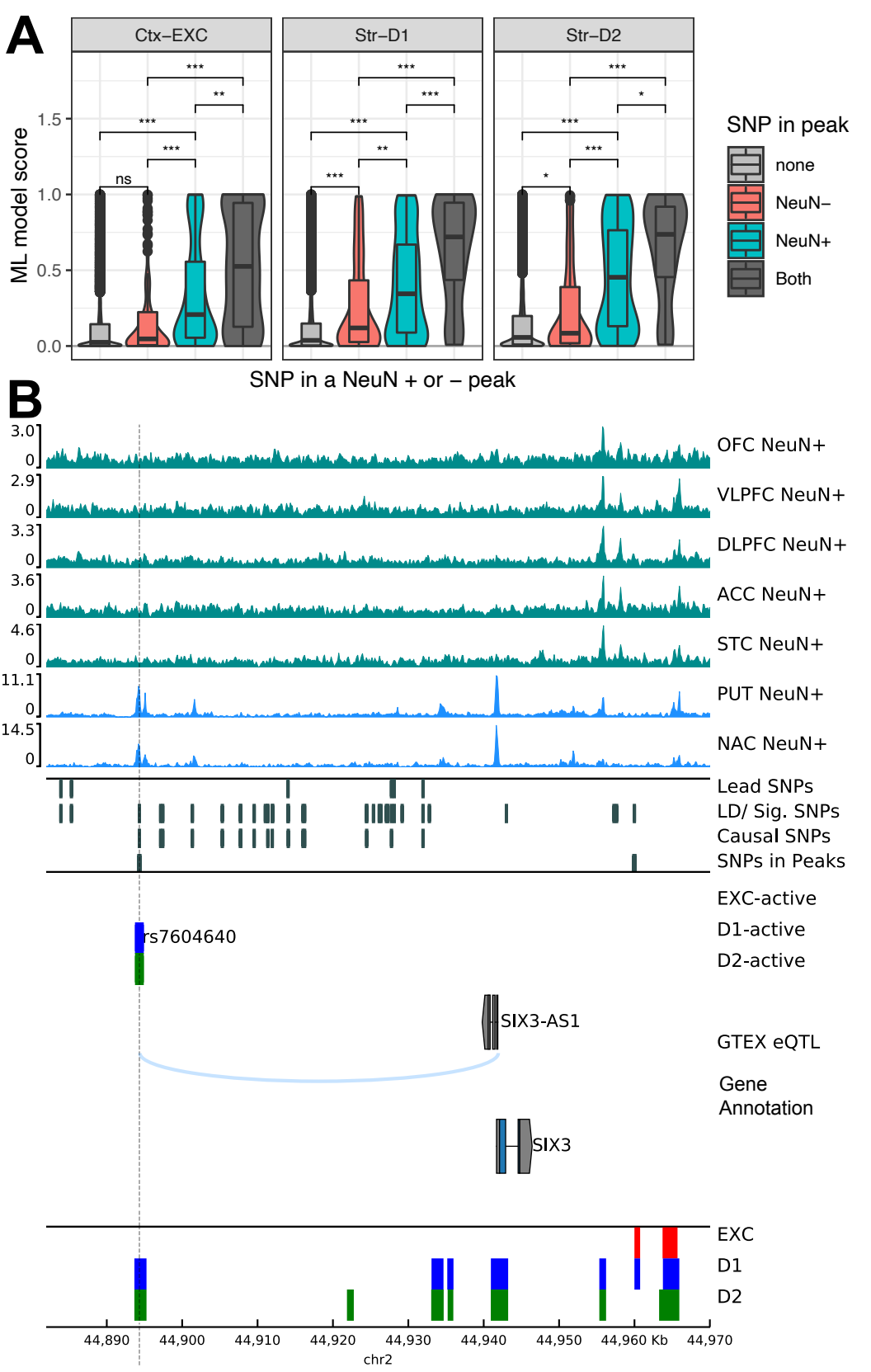
A
Ctx–EXC
Str–D1
Str–D2
ML model score
SNP in a NeuN + or – peak
SNP in peak
none
NeuN–
NeuN+
Both
B
OFC NeuN+
VLPFC NeuN+
DLPFC NeuN+
ACC NeuN+
STC NeuN+
PUT NeuN+
NAC NeuN+
Lead SNPs
LD/ Sig. SNPs
Causal SNPs
SNPs in Peaks
EXC-active
D1-active
D2-active
rs7604640
SIX3-AS1
GTEX eQTL
Gene Annotation
SIX3
EXC
D1
D2
chr2

Figure 4

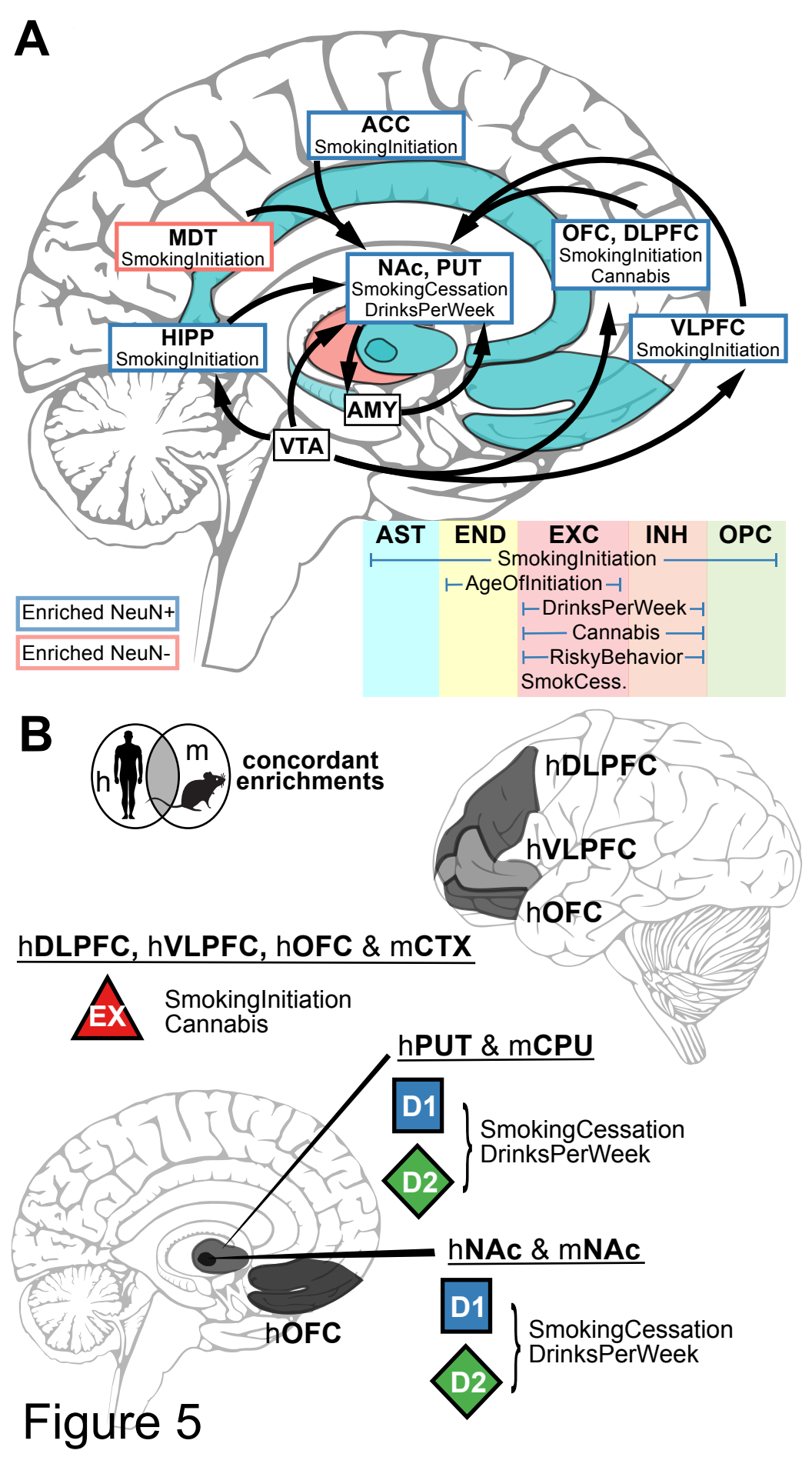
A
ACC
SmokingInitiation
MDT
SmokingInitiation
NAc, PUT
SmokingCessation
DrinksPerWeek
OFC, DLPFC
SmokingInitiation
Cannabis
VLPFC
SmokingInitiation
HIPP
SmokingInitiation
AMY
VTA
AST
END
EXC
INH
OPC
SmokingInitiation
AgeOfInitiation
DrinksPerWeek
Cannabis
RiskyBehavior
SmokCess.
Enriched NeuN+
Enriched NeuN-
B
h
m
concordant
enrichments
hDLPFC
hVLPFC
hOFC
hDLPFC, hVLPFC, hOFC & mCTX
EX
SmokingInitiation
Cannabis
hPUT & mCPU
D1
D2
SmokingCessation
DrinksPerWeek
hNAc & mNAc
hOFC
D1
D2
SmokingCessation
DrinksPerWeek

Figure 5

A

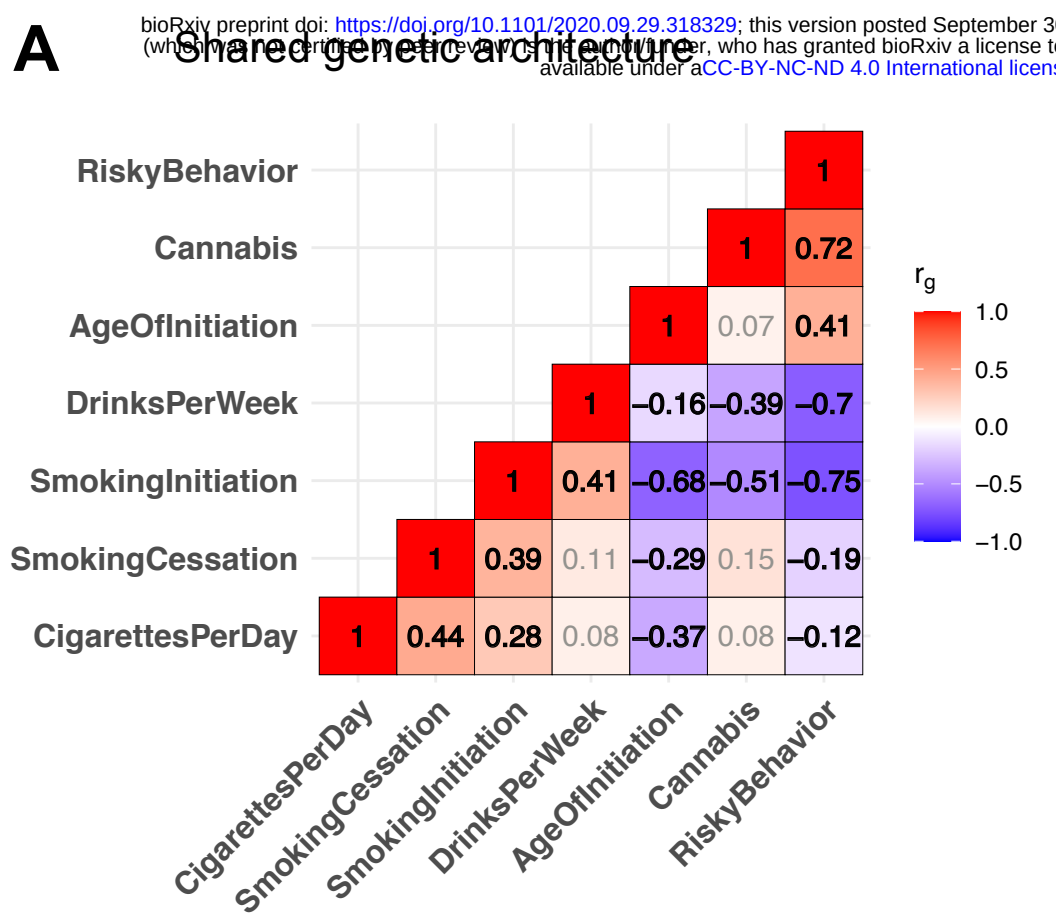

B

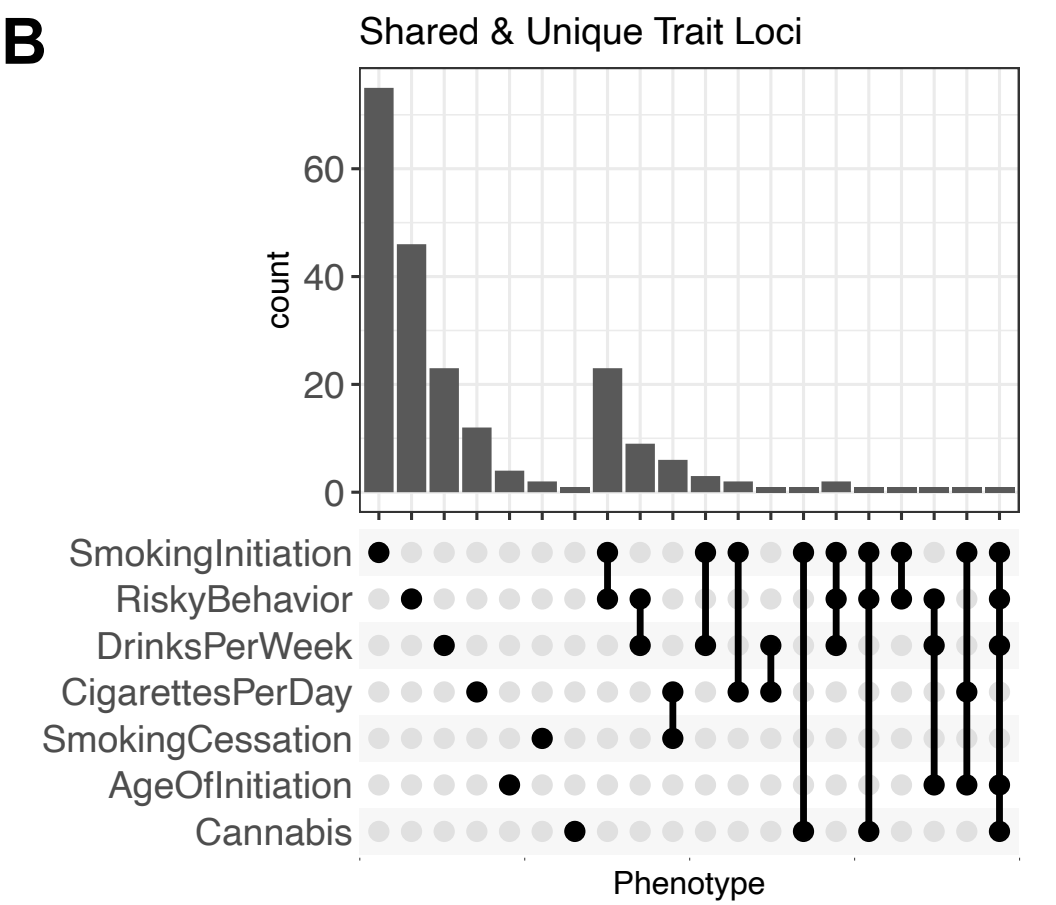

Supplemental Figure 1

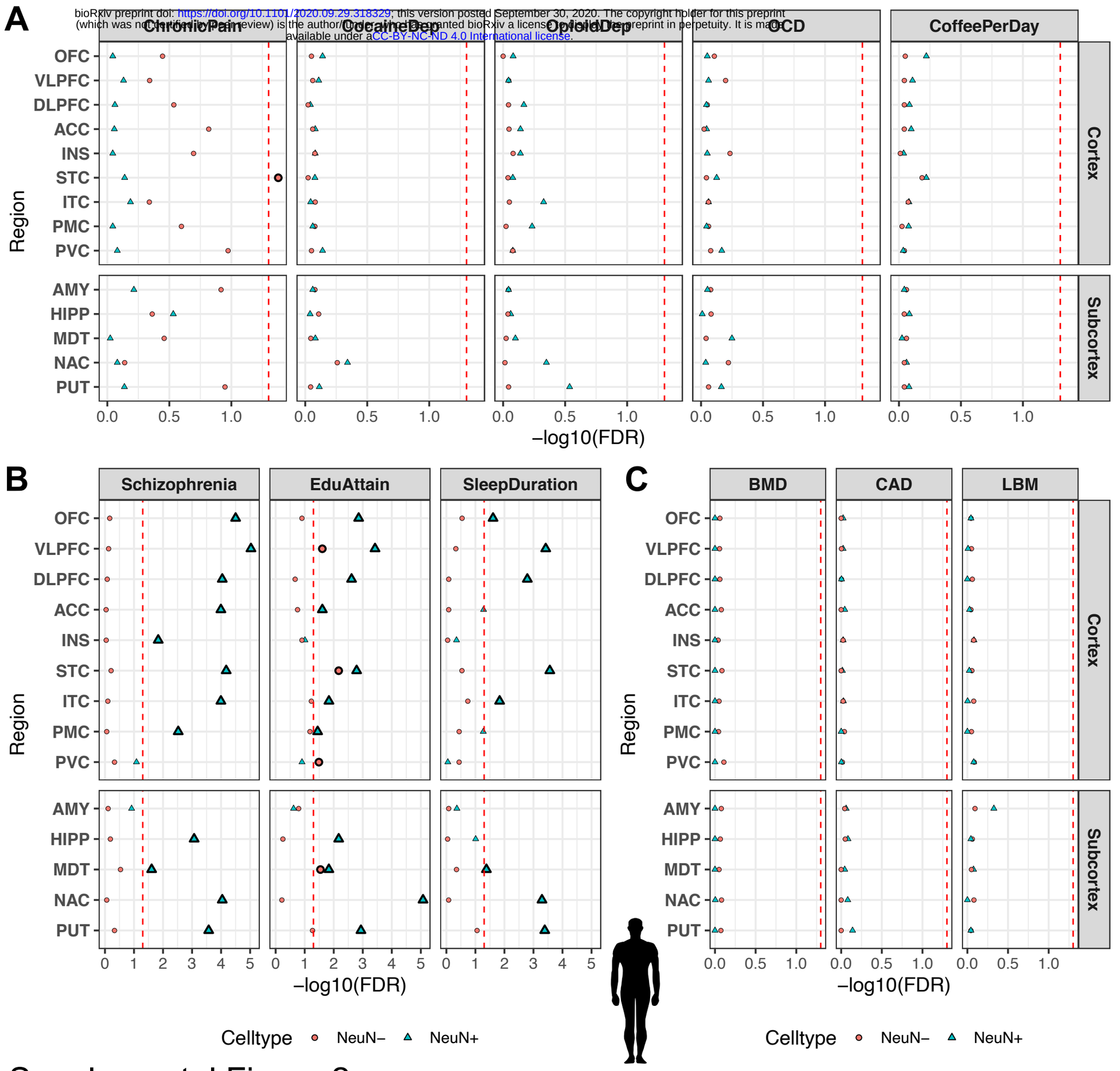

Supplemental Figure 2

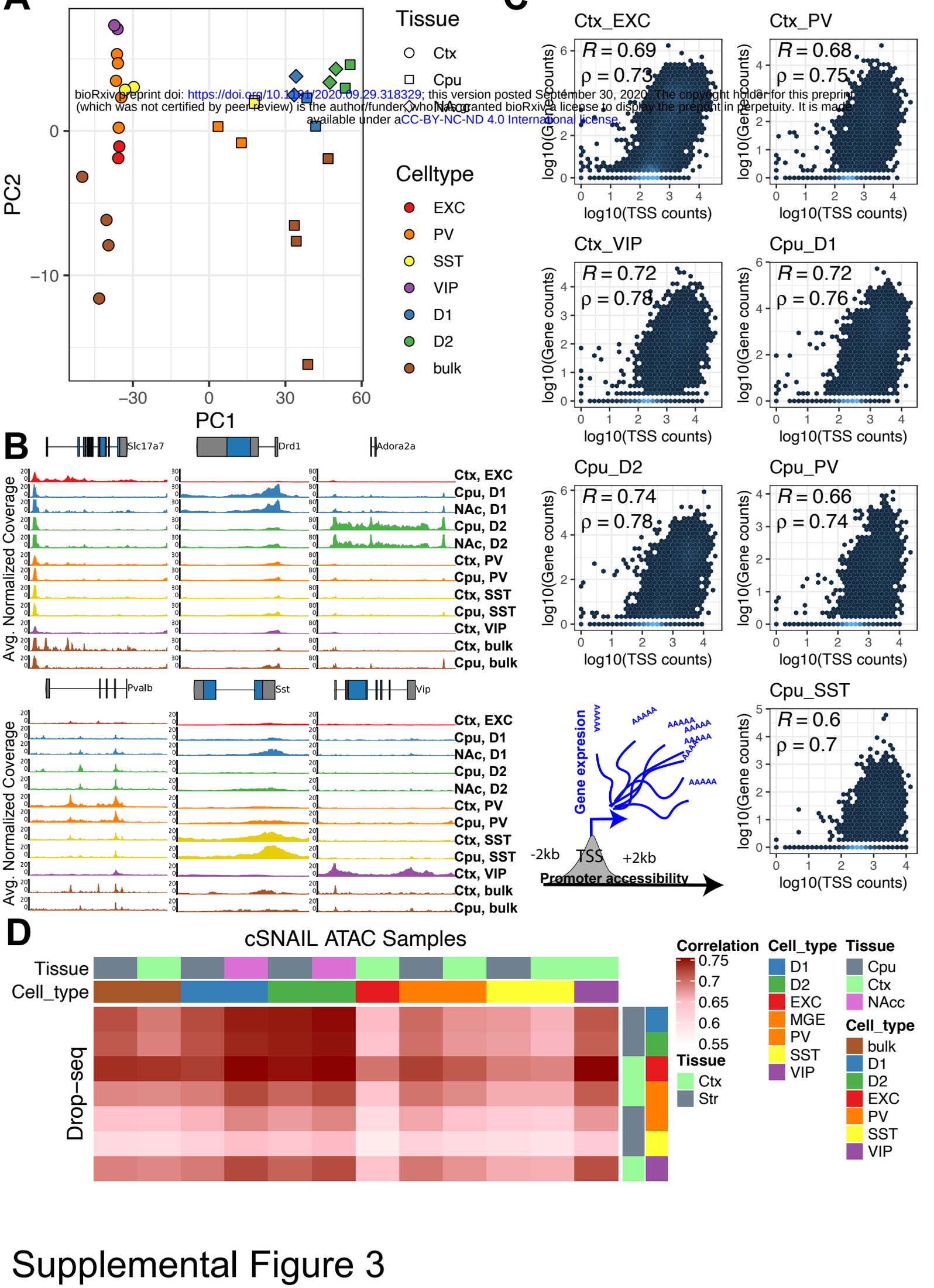

Supplemental Figure 3

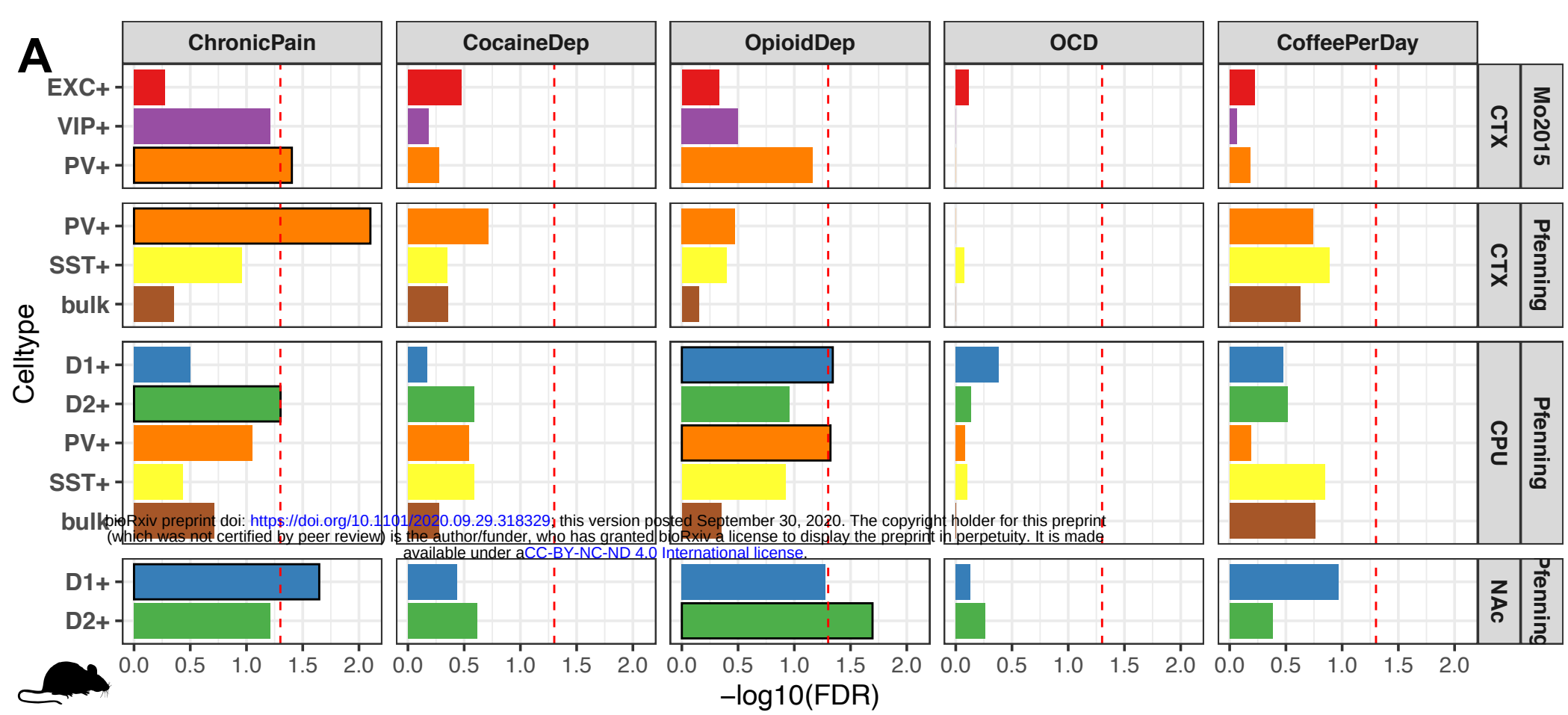

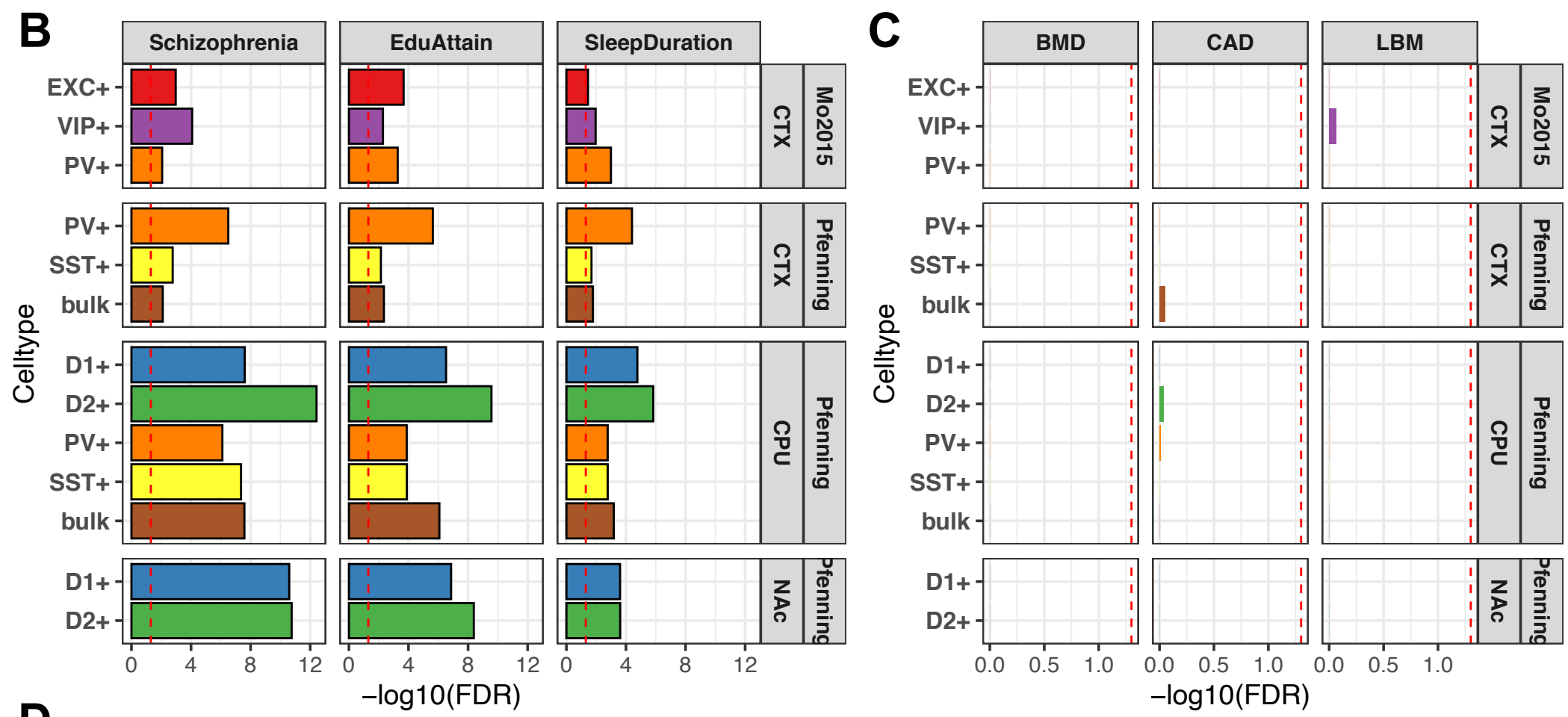

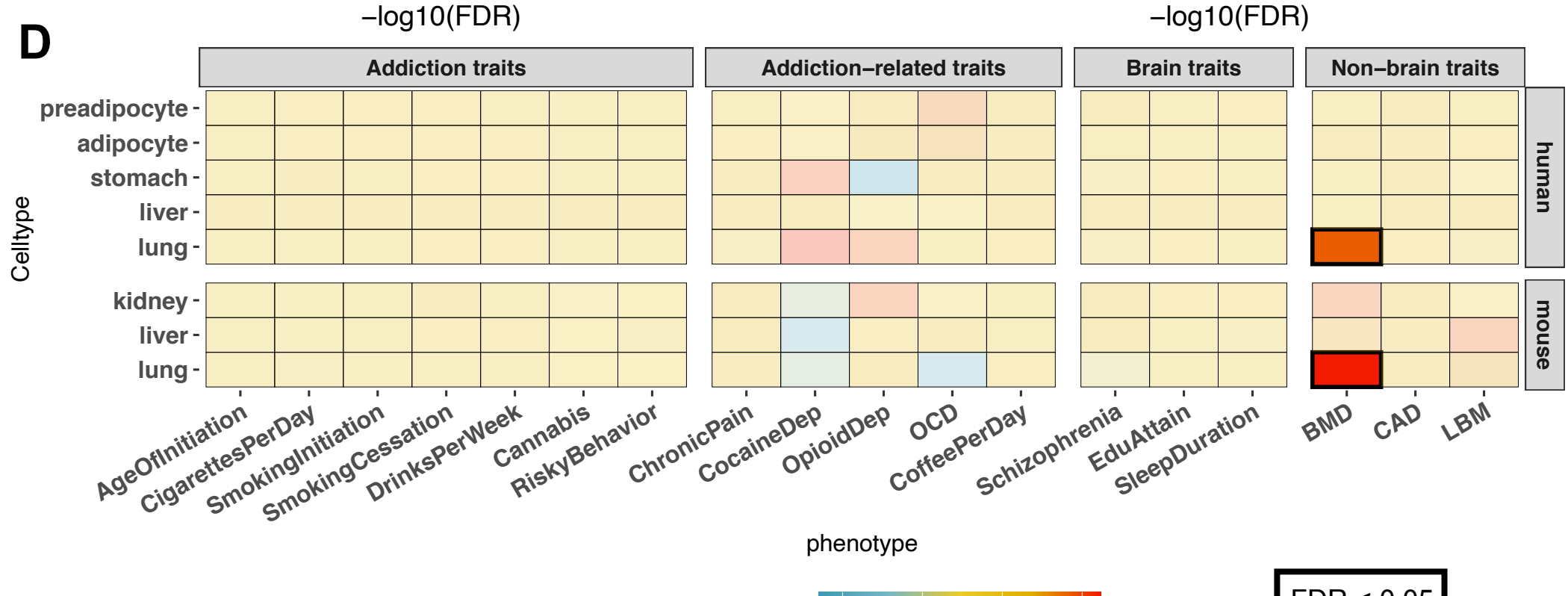

Supplemental Figure 4

A

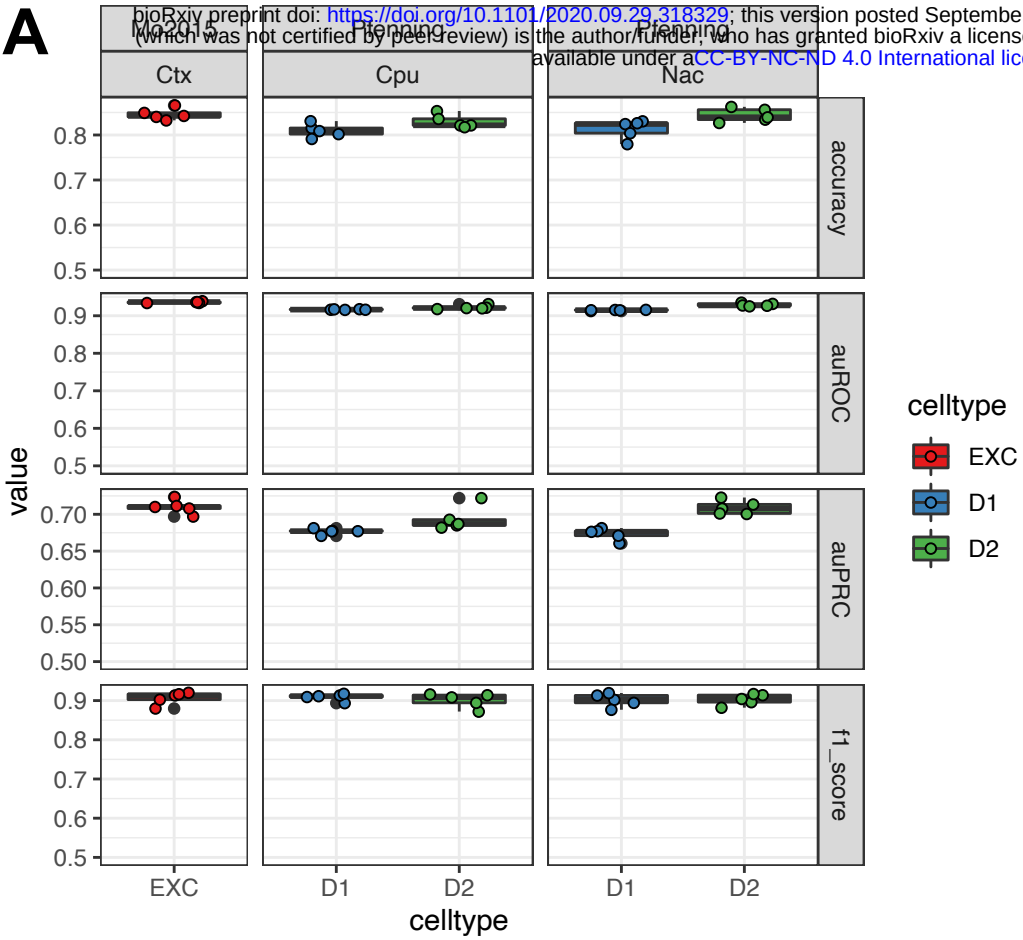

B

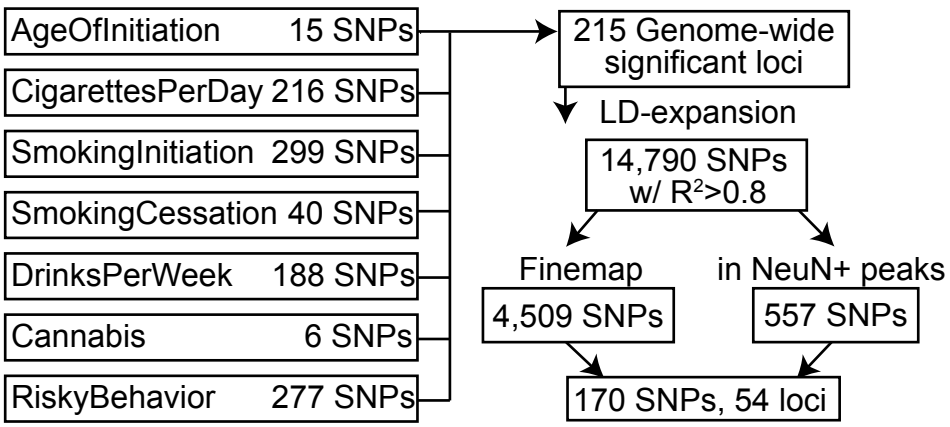

ML-predicted candidate SNP selection criteria

SNP score cutoffs:

1) in cortical or striatal NeuN+*
*depends on which ML model

2) $score_{risk\ allele} > 0.5$ or $score_{non\text{-}risk\ allele} > 0.5$

3) $delta = score_{risk} - score_{non\text{-}risk}$
$abs(delta) > 0.05$

Models:

EXC 11 SNPs

D1 12 SNPs

D2 14 SNPs

26 SNPs
16 loci

Supplemental Figure 5

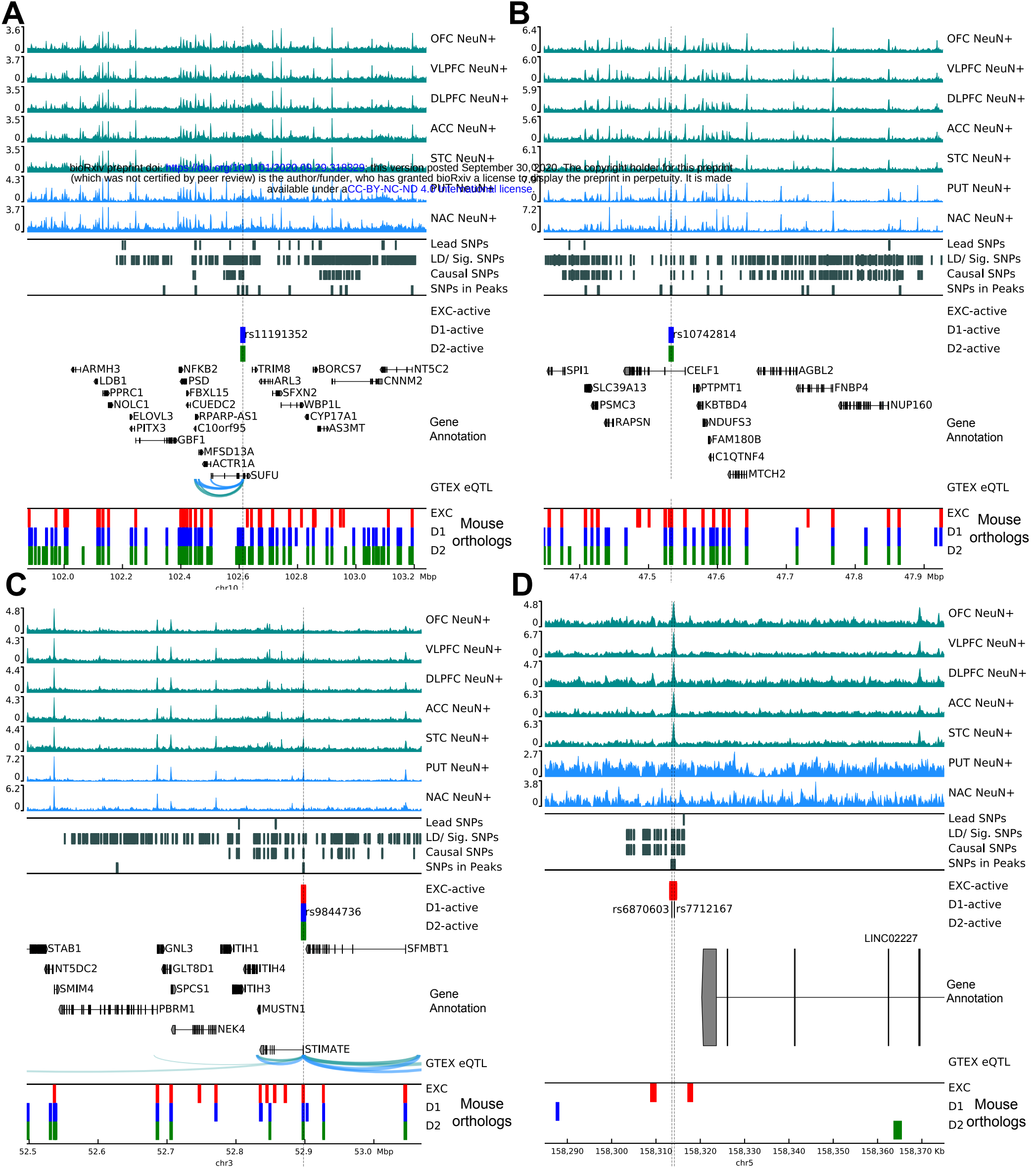

Supplemental Figure 6